Cutoff Frequencies of the Dielectrically Loaded Comb Structure as Used in Traveling-Wave Masers*

By S. E. HARRIS, R. W. DEGRASSE and E. O. SCHULZ-DUBOIS

(Manuscript received June 27, 1963)

The subject of traveling-wave maser design is reviewed and a first step towards an analytical design procedure is presented. A method is derived for calculating the upper and lower cutoff frequencies of a comb-type slow-wave structure of simple geometry. It is based on the electromagnetic field pattern and the equivalent impedances which are calculated for these frequencies, both for the dielectrically loaded and the empty comb structure. The design procedure resulting from these calculations permits the prediction of a dielectric loading geometry that shifts the upper and lower cutoff frequency of the empty comb to new, lower values which can be arbitrarily specified within certain limitations. Frequencies calculated by this procedure are compared with the results of measurements, and it is found that cutoff frequencies can be predicted to better than 10 per cent.

I. INTRODUCTION

In the early development of the traveling-wave maser (TWM),[1] the design procedures used were largely empirical. Short TWM model sections were built, tested and modified in order to meet the desired performance specifications. By this cut-and-try method, a satisfactory design was finally derived which was applied in the construction of full-length TWM's.

However, a more satisfying approach is possible if the relevant theoretical aspects regarding the maser active material, the ferrimagnetic isolator and the electromagnetic behavior of the slow-wave structure are known, either rigorously or approximately. Then a TWM can be designed on the basis of analysis before actual construction. Most attractive in the analytical approach is the inherent flexibility and versa-

* This work was supported in part by the U.S. Army Signal Corps under Contract DA 36-039-sc-85357.

tility. Thus, a large number of design ideas may be explored and a near optimum configuration can be found before any hardware is built.

The present paper is a step in the direction of a more analytical approach. Using reasonably accurate approximations to the field pattern at both cutoff frequencies, the equivalent TEM line impedances, the "effective" dielectric constants and, finally, the cutoff frequencies are calculated. This results in a numerical design procedure for the TWM structure. The analysis is made for a comb having fingers of rectangular cross section and for dielectric loading with maser material in the form of one or two rectangular parallelepipeds as shown in Fig. 1. Comparison of cutoff frequencies calculated by this method with experiment shows agreement to usually better than 5 per cent.

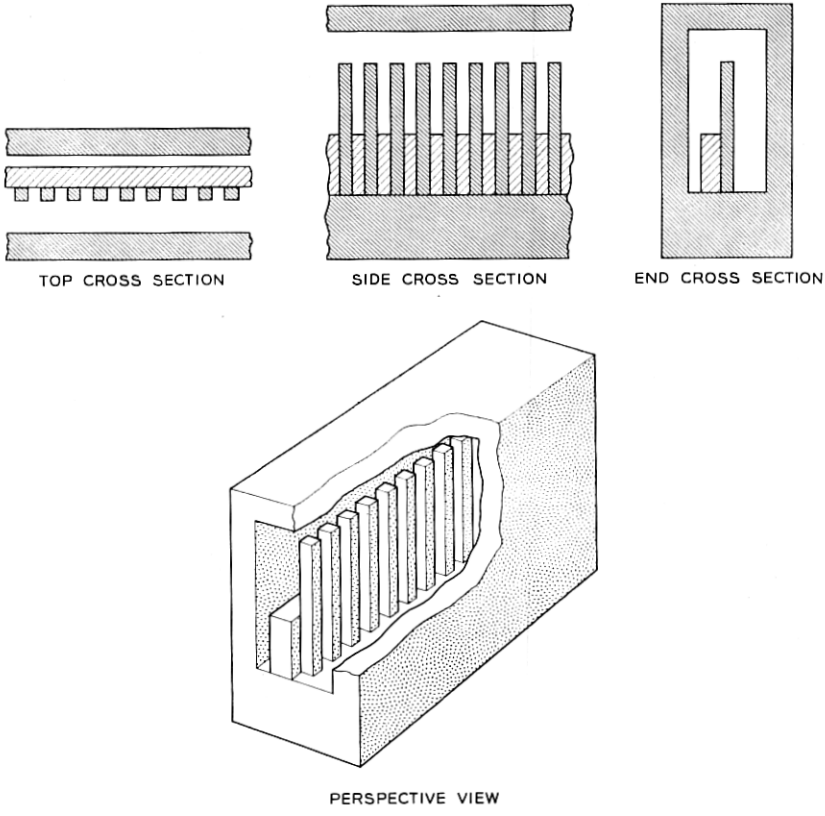

Fig. 1 — Typical comb structure.

1.1 *The Significance of Cutoff Frequencies in TWM Design*

Consider the TWM electronic gain formula[1]

$$G(\text{db}) = 27.3(-\chi'')fFl/v_g . \tag{1}$$

Here $(-\chi'')$ is the inverted susceptibility of the maser active material, f the signal frequency, F the filling factor, l the length of the maser structure and v_g the group velocity. The TWM net gain is obtained by subtracting from (1) the slow-wave structure loss (copper loss) and the ferrimagnetic isolator loss (ferrite loss).

In the development of a practical TWM, the design frequency f and the structure length l are generally determined by the application. The susceptibility $(-\chi'')$ is a property of the active material which cannot be theoretically predicted and must be experimentally determined. $(-\chi'')$ is redefined as

$$-\chi'' = I\chi_0'' \tag{2}$$

and the quantities I and χ_0'' are determined by two independent measurements. Here, I is the inversion ratio, i.e., the ratio of electronic gain from the activated maser material to electronic loss in the same material at thermal equilibrium. J. E. Geusic and W. J. Tabor have carried out inversion measurements for ruby maser material in a helix test structure, and the method and results will be described in a forthcoming paper.[2] The susceptibility at thermal equilibrium, χ_0'', is measured by standard resonance techniques[3] or may be calculated from the material composition and linewidth. In this way, $-\chi''$ can be determined to about 10 per cent, which is adequate for the present design procedure. Complications can arise in practice, however, if nominally identical crystals show variations in the active ion concentration or in the crystalline perfection.

The filling factor F may be factorized into two expressions

$$F = F_p F_v \tag{3}$$

where

$$F_p = \left[\int_M |\mu \cdot H^*|^2 \, dA\right] \Big/ \left[|\mu|^2 \int_M |H|^2 \, dA\right] \tag{4}$$

and

$$F_v = \left[\int_M |H|^2 \, dA\right] \Big/ \left[\int_A |H^2| \, dA\right]. \tag{5}$$

Here, μ is the magnetic dipole moment associated with the maser signal

transition and H is the RF magnetic field in the TWM structure. The asterisk * denotes the conjugate complex time dependence. The integration is performed in the cross-sectional plane where M denotes the cross section of the maser material and A the total structure cross section. F_p may be called the polarization efficiency factor and F_v the volume filling factor. F_p expresses the excitation efficiency of the signal transition by the RF magnetic field present in the maser material. For example, if both μ and H are of circular polarization in the same direction, then F_p is unity. Similarly, for maser material symmetrically loaded on both sides of the comb and with a circular transition perpendicular to the finger direction, a symmetry argument shows that $F_p = \frac{1}{2}$. F_v indicates what fraction of the total magnetic field energy is contained within the maser material. F_p and F_v are functions of frequency across the passband of the comb structure. Usually, however, it is sufficient to consider F at some midband frequency where it is only a slowly varying function of frequency.

Experience suggests that it is possible to estimate F to fair accuracy from the TWM geometry and a qualitative estimate of the RF magnetic field pattern. For example, it is estimated that in TWM's designed in this laboratory for 5.6, 4.2, 2.4 and 1.4 gc the filling factor F varies over the relatively limited range from 25 to 45 per cent. Thus, from the viewpoint of the analytical design of the TWM, a detailed computation of the RF magnetic field configuration is of no great value unless the other factors entering the TWM gain formula are known with comparable accuracy.

Up to the present time, this was not the case, the factor least amenable to analytical prediction being the group velocity v_g. It is well known that a wave traveling through a slow-wave structure has field components varying like $\exp [i(\omega t - \beta z)]$, where $\omega = 2\pi f$, t is the time, β the phase propagation constant and z the length coordinate along the structure. In the comb structure, each finger is an energy storage element capable of resonant storage in the same way as a quarter-wavelength coaxial resonator. As a general rule, the phase shift between adjacent elements may assume values between 0 and $\pm\pi$ as the frequency is varied across the passband. The phase shift values 0 and $\pm\pi$ are associated with the cutoff frequencies. The comb structure is normally a forward-wave structure, where $+\pi$ is the phase shift at the upper cutoff frequency and 0 that at the lower. It is possible (although not of practical importance in TWM design) to make the comb a backward-wave structure, in which case $-\pi$ is the phase shift at the lower cutoff frequency and 0 that at the upper. In the normal forward-wave comb

structure, the phase propagation constant then varies from $\beta = 0$ to $\beta = (N - 1)\pi/l$ across the passband, where N is the number of fingers and l is the structure length measured between centers of the first and last finger. The group velocity is given by

$$v_g = d\omega/d\beta. \tag{6}$$

Typical diagrams of β as a function of ω are shown in Fig. 2(a). As the curves approach the cutoff points, they assume infinite slope, corresponding to zero group velocity. There is a range at midband, however, where the group velocity is fairly constant. These graphs are typical of most of the structures studied but exceptions occasionally were found, as indicated in Fig. 2(b). These exceptions include backward-wave structures where phase and group propagation take place in opposite directions. They also include "mongrel" structures where, over part of the band, β is a double-valued function of ω; these, therefore, are forward and backward at the same time. This latter case is a very undesirable one; as discussed in Ref. 4, the existence of two propagation modes at the same frequency, one a forward wave, the other a backward wave, allows for propagation with gain in both directions despite the presence of an isolator. As a result, the maser will oscillate instead of offering stable gain. Empirically, however, this situation can be easily diagnosed and there are remedies to rectify it. Therefore, double-valued ω-β relations may be excluded from the present considerations.

With this proviso, it can be seen from Fig. 2(a) that the midband group velocity can be estimated reasonably well from a knowledge of the two cutoff frequencies alone, viz.

$$v_g = 2a\Delta f l/(N - 1) = 2a\Delta f \Delta l. \tag{7a}$$

Here Δf is the frequency width of the passband, Δl is the center-to-center spacing between comb fingers and a is a numerical factor which takes into account the detailed shape of the ω-β curve. Equation (7a) may be rearranged in terms of the group velocity slowing

$$S = \frac{c}{v_g} = \frac{1}{a}\frac{\lambda/2}{\Delta l}\frac{f}{\Delta f} \tag{7b}$$

indicating that slowing is partly a geometric effect, i.e., the compression of a half wavelength into one period of the structure, and partly the effect of compression in the frequency domain, sometimes expressed by a loaded Q. a assumes values of one for a straight line ω-β relation, 1.57 for an inverse cosine, and may in practice be as high as four for a "sagging" ω-β curve. In other words, the uncertainty in estimating the

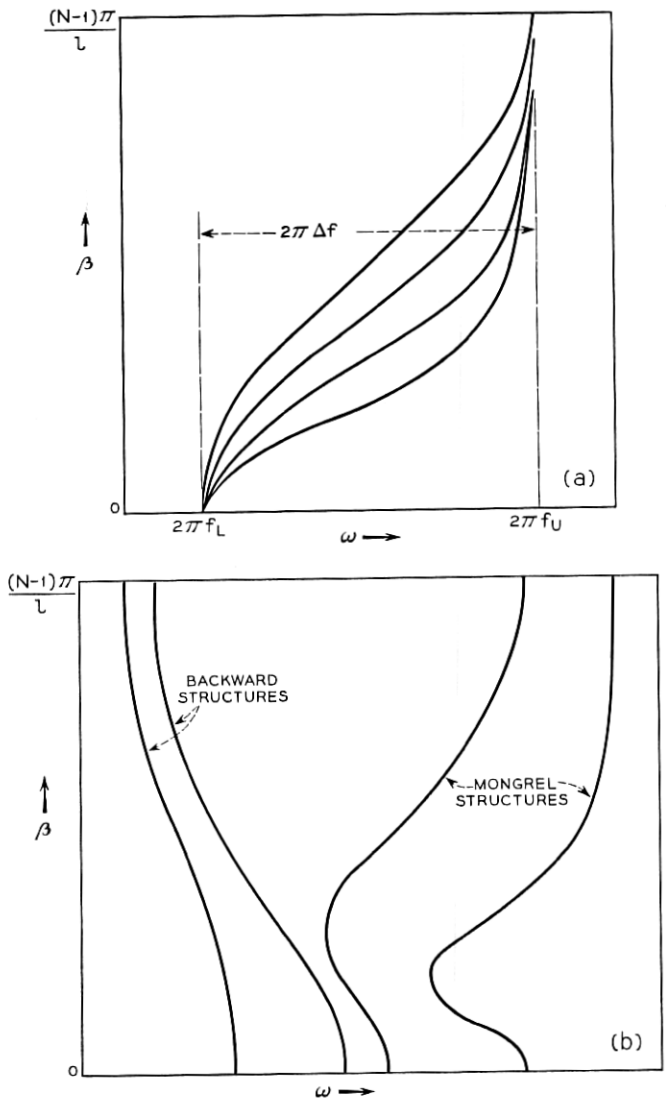

Fig. 2 —(a)Typical forward ω-β diagrams of loaded comb structures with normalized cutoff frequencies. (b) Exceptional ω-β diagrams found in comb structures with extreme dielectric loading.

group velocity or slowing from the cutoff frequencies is not very large, usually less than a factor of two.

Thus, it is clear that a method for calculating the two cutoff frequencies would be an important first step towards an analytical design procedure. Such a mathematical method should be carried out as rigorously as possible. The reason for this may be demonstrated in the following way. If fringe capacity at the finger tips and dielectric loading effects are neglected, the comb structure is electrically equivalent to the Easitron* structure. In this approximation, the comb would be a zero passband structure with identical cutoff frequencies like the Easitron. In reality, they differ only because fringe capacity and dielectric loading affect both frequencies to different degrees. Thus, the width of the passband Δf is obtained as a small difference between large numbers, the upper and lower cutoff frequencies, f_U and f_L. To obtain Δf with *fair* accuracy, f_U and f_L must be known with *good* accuracy. Similarly, a small change in the dielectric loading may change f_U and f_L each by a small percentage, but Δf by an appreciable factor. Experience has shown that comb structures with different dielectric loadings may have a passband width Δf anywhere between 1 and 50 per cent of the midband frequency. In other words, as long as the cutoff frequencies are not known, the uncertainty in an estimate of v_g may be almost two orders of magnitude. The computation of the cutoff frequencies would be very useful if it could reduce this uncertainty to about a factor of two. Besides determining the group velocity and hence, indirectly the electronic gain, the cutoff frequencies also define the center frequency and the tunable bandwidth of the TWM. Since it is impossible to match a structure right up to the cutoff frequency, the useful tunable band is well inside the structure passband Δf. An analytical design procedure that allows a reasonably accurate prediction of the cutoff frequencies would clearly be desirable, as center frequency and tunable bandwidth are among the primary TWM specifications.

1.2 *The Function of Slow-Wave Structures in Electron Beam Tubes and TWM's*

A considerable amount of work, both theoretical and experimental, has gone into the study of slow-wave structures for tubes. It would be gratifying if this knowledge could be used in TWM work. Unfortunately,

* The Easitron was analyzed by L. R. Walker, unpublished manuscript, quoted in Ref. 1. This structure consists of a rectangular waveguide with an array of uniform, identical conductors in the H plane connecting both short walls. It has zero passband, nonpropagating resonances of frequencies where the conductor length is one or more half wavelengths.

this work has only limited applicability to the TWM. This is more readily understood if slow-wave structures for electron beam tubes and for TWM's are compared.

In tubes, slowing factors between 10 and 100 are typical, while in the TWM, slowing of 50 to 1000 is used. This difference influences primarily the mechanical tolerances, which are tighter for higher slowing.

A more fundamental distinction concerns the applicable slowing concept. In an electron beam tube there must be synchronism between the electromagnetic mode propagated on the slow-wave structure and the interacting mode characterized by a charge distribution on the beam. Therefore, the analysis of tubes is concerned with the phase velocity of the slow-wave structure mode. Similarly, in a traveling-wave parametric amplifier there must be synchronism between pump, idler and signal propagation, requiring a phase velocity relation for these three frequencies. In filter circuits the condition of synchronism is usually satisfied only over a small fraction of the total structure bandwidth. By contrast, the amplification by the maser material does not depend on the existence of phase relations along the TWM structure. The maser material may be considered as an incoherent, long-time energy reservoir from which energy is withdrawn upon stimulation by an incident signal and added to the incident signal in a coherent phase preserving fashion. The function of the slowing is merely to "give the signal more time" to interact with the energy stored in the maser material, i.e., to enhance the stimulating gain interaction. Thus, the analysis of TWM's is concerned with the signal group velocity in the structure rather than phase velocity. It is not necessary that v_g be constant over the tunable band. If the gain over the tunable band is required to be constant, then the product $-\chi'' F f/v_g$ (neglecting copper and ferrite losses) should be constant over the band. Experience has shown that this condition can be met over almost the entire passband.

Another point is the interaction mechanism between the active element and the slowing structure. An electron beam interacts with a structure mode via the RF electric field, and the interaction is conventionally represented by an interaction impedance. The interaction of the inverted spins in the maser material with the structure mode takes place via the RF magnetic field, and its strength is measured by the filling factor.

All the differences mentioned have no bearing on the question whether the knowledge of slow-wave structures accumulated in studies directed towards electron beam interaction can be applied to TWM structures. For example, the degree of slowing is not essential for a theoretical anal-

ysis, the group slowing is easily derived by differentiation from the phase propagation, and electric and magnetic interaction terms can be obtained equally well from the field analysis.

The chief difference in slow-wave structures for these two applications lies in their relation to dielectric loading. In a tube, dielectric loading is undesirable and is usually avoided as far as possible. By virtue of its dielectric constant, the glass envelope of a TWT, for example, drags away from the beam some of the electric field energy carried by the helix and thus reduces the gain interaction. In fact, most studies of slow-wave structures for beam tubes pertain to metal structures surrounded by vacuum.

Dielectric loading, being an undesirable side effect for tubes, is an essential and rather beneficial feature in maser structures. Since the gain interaction is magnetic in nature, the interaction of the electric field with dielectrics may be used to advantage without deteriorating the gain interaction. Indeed, it is being used for reducing the over-all maser size, tuning the band center frequency, adjusting the tunable bandwidth or increasing the gain by increased slowing (of course, the items mentioned are not independent). Thus, a high degree of design flexibility can be obtained, even with the identical copper comb, merely by changing the dielectric loading.

For this reason, dielectric loading must be included in any treatment of TWM structures. The present paper is a first contribution to the theoretical treatment of maser structures taking dielectric loading into account. To keep the mathematics reasonably simple, the maser comb geometry, including the dielectric loading, was chosen to be fairly simple. In the laboratory, dielectric loading techniques were developed in which the loading consists of more than one dielectric and has more complex shapes. Work to be published by F. S. Chen has generalized the analysis to take these modifications into account. It also expands the present analysis of the cutoff frequencies into a more general one which allows the prediction of the entire ω-β diagram. This will be particularly valuable in finding criteria to avoid structures having a double-valued "fold-over" or "mongrel" ω-β diagram.

II. GENERAL PROBLEM AND APPROACH TO SOLUTION

The problem is to find by analysis the upper and lower cutoff frequencies of the comb-type slow-wave structure as used in a traveling-wave maser (TWM). In particular, this implies taking into account the dielectric effect resulting from loading the comb with maser material or

possibly some other dielectric material and the effect of the fringe capacity at the tips of the comb finger. It was pointed out before that, in a zero-order approximation neglecting both effects, the comb is a zero passband structure.

In the course of this treatment it will be necessary to introduce a number of restrictions and approximations. These are mostly required in order to keep the mathematics manageable. Some other restrictions are introduced in order to have the geometry underlying the calculations correspond to the type of TWM geometry which is presently investigated in the laboratory. These various restrictions and approximations are labeled with lower-case roman numerals for reference in this discussion.

(*i*) *The first restriction pertains to the cross section of the comb fingers. The treatment used here is applicable only to combs with fingers of rectangular cross section.*

This means that it is not possible to apply this type of analysis to a comb having round fingers as used in the original TWM's. It may be mentioned here, however, that it is possible to treat the round-finger comb as long as certain simple frequency or impedance data are available from measurements on scale models, resistance cards or measurements in the electrolytic tank.

Besides being better suited for mathematical analysis, there is another justification for treating combs with rectangular fingers. This has to do with fabrication of combs. There is indication that it is possible to fabricate combs with rectangular fingers not only with greater ease but also with greater perfection. The subject of these fabrication techniques may be discussed at some later date.

A typical comb structure as treated here is shown in Fig. 1. The fingers shown are of square cross section and are spaced by a finger width. It should be emphasized that the general method used here is applicable to any rectangular cross section and spacing, although a great many of the computations are concerned with square fingers spaced by a finger width.

(*ii*) *The next restriction is that maser material (or some other dielectric) is inserted into the comb in the shape of a single rectangular parallelepiped.*

The restriction to parallelepipeds is rather definite. There is a possibility, however, of considering more than one slab of maser material loading the comb. No change in the general analysis is required if two identical slabs are considered which are loaded symmetrically on both sides of the comb. This is shown in Fig. 3(a). The analysis could be carried out also for the case shown in Fig. 3(b) where the maser material is in-

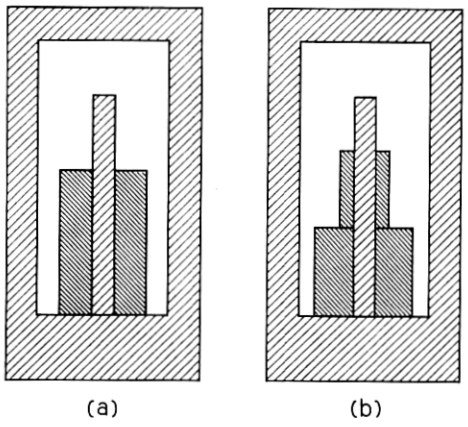

Fig. 3 — Loading geometries.

serted in the form of two pairs of identical slabs. It should be mentioned, however, that the calculation will be appreciably more cumbersome in this case. Although it will not be described in detail, it will be fairly obvious to the reader how the calculations have to be modified to take into account geometries like the one of Fig. 3(b).

(iii) A further simplifying assumption is that the dielectric loading is assumed to have an isotropic dielectric constant, at least for field components perpendicular to the finger direction.

This assumption is not too restrictive. An effective dielectric constant may be estimated in the case of a tensor dielectric constant. This estimate will usually be different for either cutoff frequency, since it depends on the electric field configuration. As the tensor components are always of the same order of magnitude, the estimated effective dielectric constant should turn out to be sufficiently accurate for most cases of practical interest.

No provisions have to be made for magnetic permeability. Outside the maser signal line, $\mu' = 1$ for the maser material. Even within the frequency range of the signal line, the deviation of μ' from unity is so small that it can be neglected for all practical purposes as a factor influencing the cutoff frequencies. A similar reasoning applies to the ferrimagnetic isolator. Even though the values of $\mu' - 1$ are larger there, they are less effective due to the very small ferrimagnetic filling factor.

The starting point for the calculation is the phase shift. At one cutoff frequency the phase shift between fingers is zero. This has the consequence that an instantaneous electric field pattern within the comb may

look like Fig. 4(a). Usually, although not necessarily so, this is the case at the lower cutoff frequency, f_L. Throughout the paper this case will be referred to as the "lower cutoff," although the term "zero phase shift case" would be more appropriate. The field pattern is repetitive and shows no field lines from finger to finger since they are on the same potential. It is symmetric with respect to a cross-sectional plane in the structure which contains either the center line of a finger or the center line in the space between two fingers. Therefore the same field pattern is obtained with a single finger if the section of the comb containing this finger is enclosed by a "magnetic wall." A magnetic wall is a fictitious plane on which the electromagnetic field components obey boundary conditions such that the electric field is tangential and the magnetic field normal to the plane. These boundary conditions are opposite from those on a perfect conductor. The perfect conductor is closely approximated

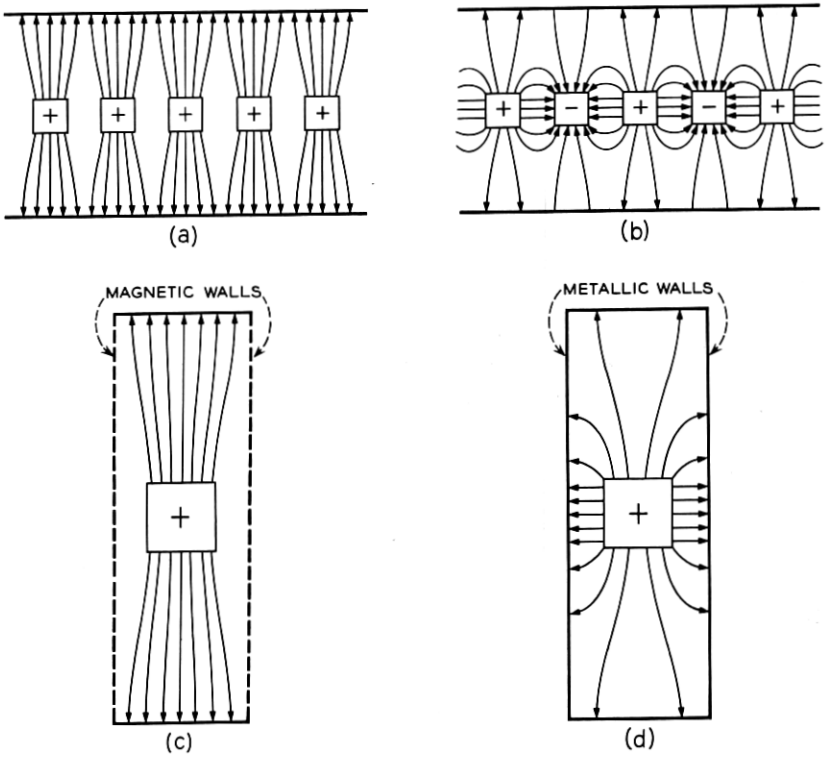

Fig. 4 — Field patterns showing phase shift conditions.

in experiments by high-conductivity metals, whereas the magnetic wall is a mathematical model only. Since the field patterns of Figs. 4(a) and 4(c) are identical, the frequencies will be the same, too. Thus the lower cutoff frequency of the comb can be found as the resonant frequency of the one-finger structure in Fig. 4(c).

A similar reasoning applies to the upper cutoff frequency f_U. Here the phase shift is π between adjacent fingers. An instantaneous field pattern will therefore look like Fig. 4(b). Since adjacent fingers are subject to opposite potential, there are strong electric field components going from finger to finger. The field pattern is symmetric with respect to a cross-sectional plane in the structure which contains the center line of a finger, but antisymmetric with respect to a cross-sectional plane which contains the center line in the space between two fingers. Thus the same field pattern can be realized on a single finger if the section of the comb containing the finger is enclosed by a perfectly conducting (or metallic) wall. This wall will take the place of the plane of antisymmetry in the comb. This is illustrated in Fig. 4(d). Again, identical field patterns require the same frequency. Thus the upper cutoff frequency of the comb can be found as the resonant frequency of the one-finger structure in Fig. 4(d).

The method of determining the resonance frequency of either one-finger model, that of Fig. 4(c) or 4(d), is suggested by Fig. 5. The finger acts essentially as a quarter-wave TEM resonator. At the comb base, this TEM line is terminated in a short. At the finger tip the TEM line is terminated by a nearly perfect "open." This is only slightly modified by fringing electric fields between the finger tip and the surrounding walls. The effect of these fields can be lumped into a fringe capacity C. In principle, C will be different for both cutoff frequencies.

Unfortunately, both capacities C_U and C_L cannot be calculated easily. Therefore, measurements have been made in an analog electrolytic tank setup. A scale model having the cross section of the one-finger lines in Figs. 4(c) and 4(d) was built. This cross section is shown in Fig. 6(a) for the upper cutoff frequency and in Fig. 6(b) for the lower. In the electrolytic tank the electric field lines of the object under study are simulated by the current lines in the tank fluid. No approximation is involved in this analogy. In particular, it is possible to simulate a magnetic wall like that of Fig. 3(c) by an insulating wall. This is done in the cross section used in the lower cutoff analog measurement shown in Fig. 6(b). In the analog measurements, the metal configuration was first lowered to the insulating bottom of the tank as indicated in Fig. 6(c). The resistance measured between electrodes in this fashion is proportional to the impedance of the corresponding TEM mode of the one-finger line; it is

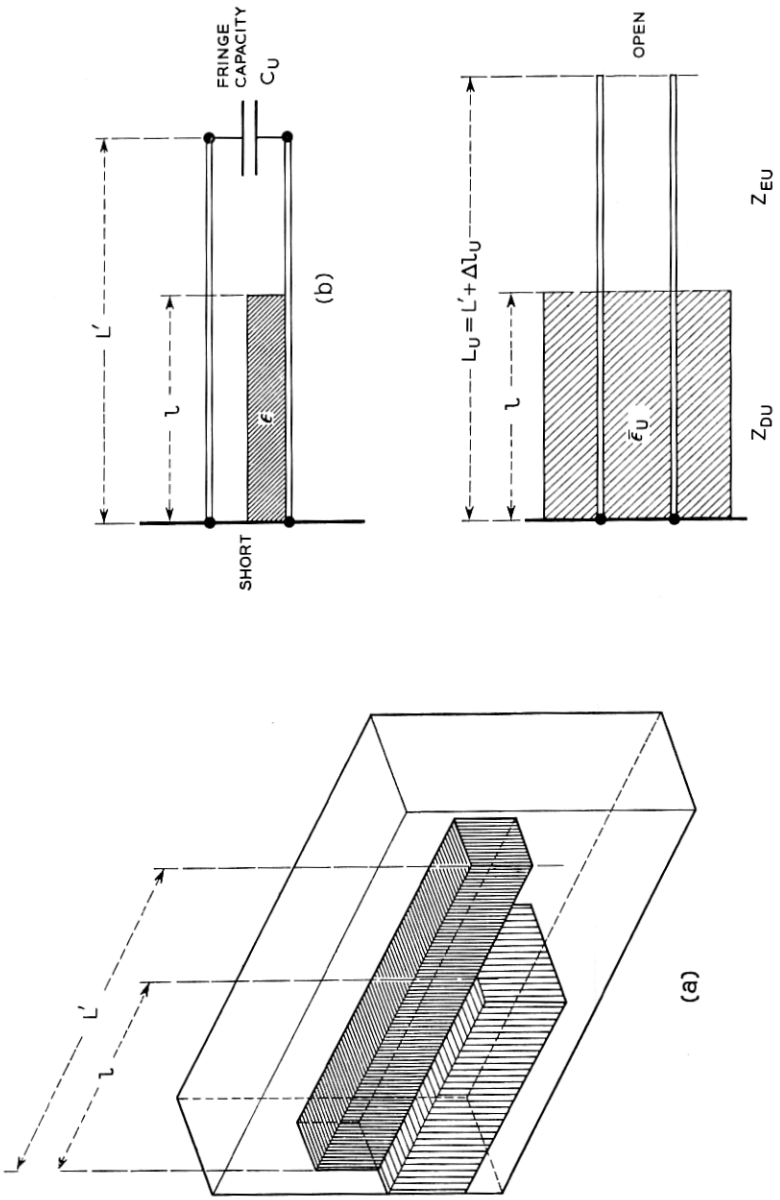

Fig. 5 — Equivalent one-finger line: (a) geometry considered, (b) two-wire line model, (c) simplified equivalent TEM mode line model; use either subscript U for upper, or L for lower, cutoff.

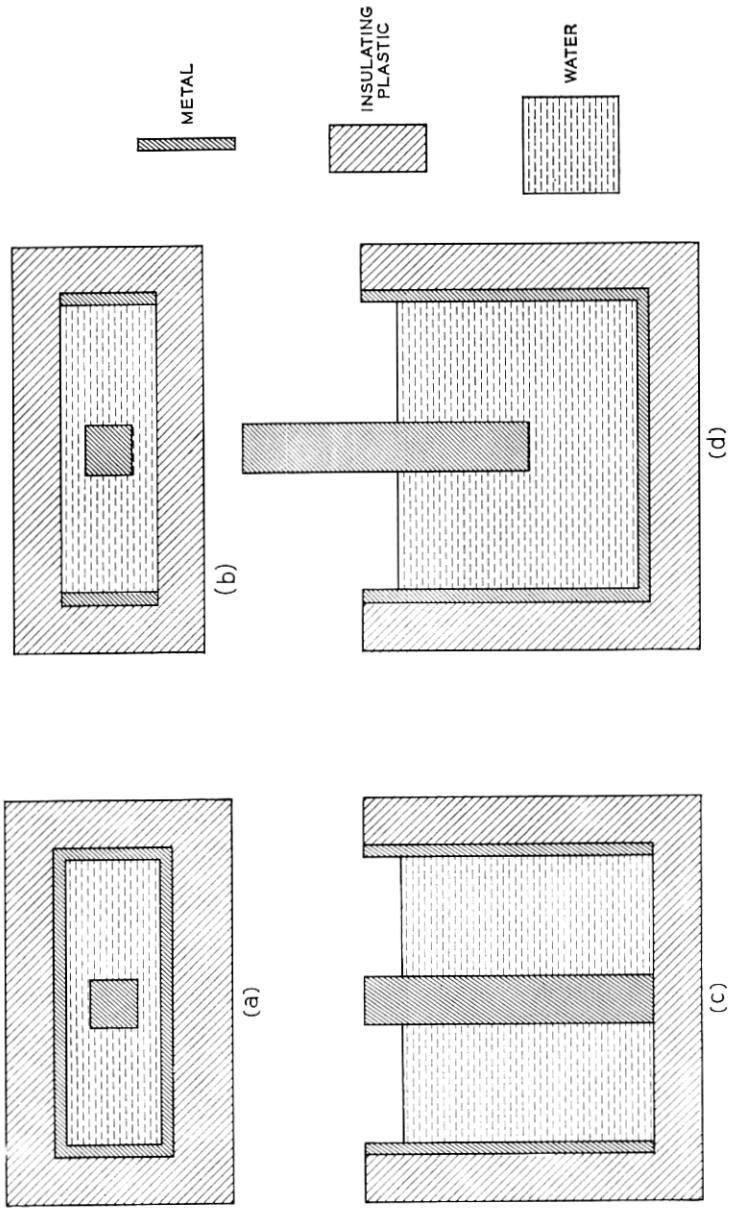

Fig. 6 — Electrolytic tank measurements.

inversely proportional to the capacitance of the line. For a second measurement, the finger was raised to the proper scaled height and a metal plate was placed on the bottom of the tank. The inverse of the resistance so measured is proportional to the capacity of the appropriate length of one-finger TEM line plus the fringe capacity arising from the diverging field pattern beyond the end of the finger. [See Fig. 6(d).] The conductivity of the tap water used was measured also. From these measurements it is possible then to evaluate the fringe capacity as well as impedance and capacitance of the TEM mode on the one-finger line.

In Fig. 7, the fringe capacitance values C_L for the lower cutoff frequency and C_U for the upper cutoff frequency obtained from the tank

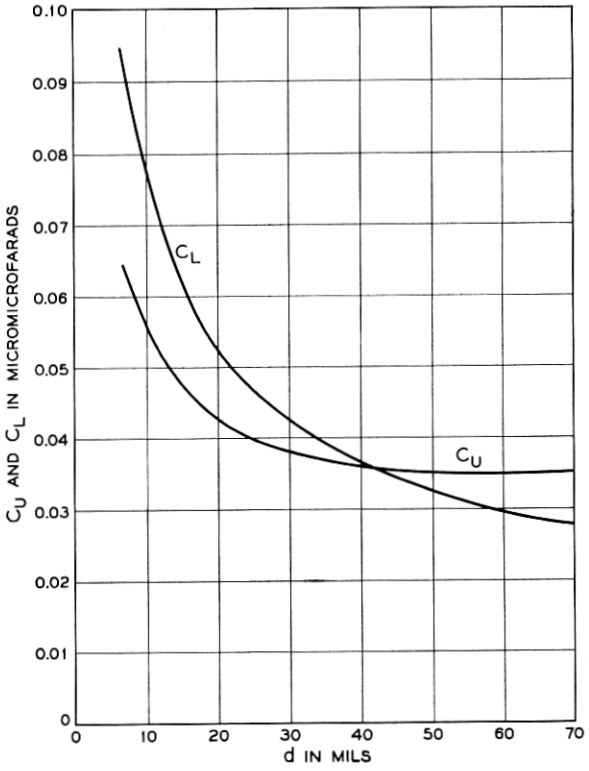

Fig. 7 — Fringing capacitance C_L for lower cutoff frequency and C_U for upper cutoff frequency. The geometry of the comb used includes fingers of cross section 0.040 x 0.040 inch, spaced 0.080 inch on center in a housing 0.240 inch wide (ratio $W_U/D_U = 1.25$). Capacitance is plotted vs spacing d between finger tips and the opposing housing wall.

measurements are shown as a function of the distance d between the finger tips and the opposite waveguide wall. The data are valid for fingers of square cross section, $D_U/2 \times D_U/2 = 0.040 \times 0.040$ inch, spaced center-to-center by $D_U = 0.080$ inch and contained in a housing of width $2W_U + D_U/2 = 0.240$ inch (aspect ratio $W_U/D_U = 1.25$). The W_U and D_U are the dimensions of the empty comb, as shown in Fig. 9 in Section III. It should be mentioned here that these data can be applied to dimensions other than those indicated if one observes two facts. First, if all linear dimensions are scaled simultaneously by some factor, the capacity is scaled by the same factor. Second, experience has shown that the fringe capacity is a very slow function of the ratio W_U/D_U; no noticeable errors were found when these capacity values were used for W_U/D_U values ranging from 0.75 to 1.5.

Another experimental method to determine the fringe capacity is based on the availability of either a comb structure of exact size or a scale model. The upper and lower cutoff frequencies, f_{EU} and f_{EL}, of the empty, unloaded structure are measured by direct measurement. The result of the measurement can best be expressed in terms of a new effective finger length, L_U or L_L. This is based on the fact that a transmission line of physical length L', shorted at one end and terminated with a small capacity at the other, is electrically equivalent to a somewhat longer transmission line which is shorted at one end and open at the other. The effective finger lengths are different for both cutoff frequencies

$$L_U = \frac{c}{4f_{EU}} = L' + \Delta l_U \tag{8a}$$

$$L_L = \frac{c}{4f_{EL}} = L' + \Delta l_L. \tag{8b}$$

Here c is the velocity of light.

The relation between these length dimensions and the fringe capacity involves the characteristic impedance of the line. The fringe capacity follows from

$$\frac{1}{2\pi f_{EU} C_U} = Z_{EU} \tan \frac{2\pi f_{EU} L'}{c} = Z_{EU} \cot \frac{2\pi f_{EU} \Delta l_U}{c} \tag{9a}$$

and

$$\frac{1}{2\pi f_{EL} C_L} = Z_{EL} \tan \frac{2\pi f_{EL} L'}{c} = Z_{EL} \cot \frac{2\pi f_{EL} \Delta l_L}{c}. \tag{9b}$$

For the particular structure geometry investigated here in detail, the fringe capacity was determined using these equations and the characteristic impedances derived later in this section. The values of C_L and C_U obtained agree well with these from the tank measurement.

For the subsequent calculations it is assumed that the new effective lengths, L_U and L_L, are known. If, instead, the fringe capacities, C_U and C_L, are known, the new effective lengths can be calculated using the impedances Z_{EU} and Z_{EL}. Since the capacities are small, (9a) and (9b) can be approximated by

$$\Delta l_U = Z_{EU} C_U c \tag{10a}$$

$$\Delta l_L = Z_{EL} C_L c. \tag{10b}$$

In this fashion, the problem of Fig. 5(b) is reduced to that of Fig. 5(c). The cutoff frequencies, f_L and f_U, are found as resonance frequencies of a transmission line L_L or L_U long, where one end is shorted, the other open, and a length l is partially loaded with dielectric.

The field pattern in the unloaded part of the transmission line is rigorously a TEM mode. Therefore, the impedance of this line can be found by a resistance card or an electrolytic tank technique. The electrodes are shaped for the model in the same way as the conductors in the unloaded TEM line. Then the impedance of the line is simply equal to the resistance measured in the model provided the resistance per square is adjusted to or scaled to 377 ohms. In addition to this measuring technique, these impedances, Z_{EU} and Z_{EL}, will be determined analytically below. This involves a calculation with good accuracy of the electric field pattern.

The dielectrically loaded section of the transmission line would, if treated with the same rigor, require a much more involved procedure. Therefore, at this point an approximation is introduced.

(*iv*) *The field configuration in the loaded part of the transmission line can be treated as a TEM mode.*

In reality, this is not true. An exact solution of Maxwell's equations for a TEM-type transmission line having a cross section partly filled with dielectric is not a TEM mode. Instead, the process of matching boundary conditions requires the presence of longitudinal field components. It can be seen, however, that these longitudinal components will become smaller with decreasing frequency and vanish in the zero frequency limit. Thus this approximation implies the representation of a dynamic field configuration by its static analog. The accuracy of such an approximation, therefore, tends to be better the shorter the linear dimensions involved are with respect to the wavelength. In the range of

dimensions used here it is expected that no appreciable loss of accuracy is incurred in this connection.

The consequences of treating the field configuration in the loaded part of the one-finger model as a TEM mode are far-reaching and very helpful for the subsequent analysis. Considering the same metal boundaries as in the unloaded part, the field configuration in the loaded part has to be the same. This follows from the fact that the TEM fields are given as a unique solution to Laplace's equation for the appropriate geometry. Thus one way to treat the loaded part of the one-finger model, consistent with a TEM mode in the same geometry, is by an effective dielectric constant. This allows for a reformulation of approximation (*iv*):

The part of the transmission line loaded partially by a high dielectric constant material can be treated as if it were loaded uniformly throughout the cross section with a material of a lower "effective" dielectric constant.

This effective dielectric constant will, of course, be different for the upper and lower cutoff frequencies. Using these effective dielectric constants, $\bar{\epsilon}_U$ and $\bar{\epsilon}_L$, the impedances and propagation constants of the loaded section are related to those of the empty section by

$$Z_{DL} = Z_{EL}/\sqrt{\bar{\epsilon}_L} \qquad Z_{DU} = Z_{EU}/\sqrt{\bar{\epsilon}_U} \tag{11}$$

$$\beta_{DL} = \sqrt{\bar{\epsilon}_L}\,\beta_{EL} \qquad \beta_{DU} = \sqrt{\bar{\epsilon}_U}\,\beta_{EU}\,. \tag{12}$$

Here the first indices E and D refer to the empty and dielectrically loaded line, the second indices L and U to the lower and upper cutoff frequencies. The propagation constants in the empty TEM line are, of course, identical to that in vacuum

$$\beta_{EL} = (2\pi f_L/c) \qquad \beta_{EU} = (2\pi f_U/c). \tag{13}$$

Assuming for the moment that the effective finger lengths, L_U and L_L, the characteristic impedances of the empty line, Z_{EU} and Z_{EL}, and the effective dielectric constants, $\bar{\epsilon}_U$ and $\bar{\epsilon}_L$, are known, the cutoff frequencies, f_U and f_L, can be calculated. The procedure is to match voltage and current at the boundary between the loaded and unloaded section of the line. This results in impedance equations

$$Z_{EU} \cot \beta_{EU}(L_U - l) = Z_{DU} \tan \beta_{DU} l \tag{14a}$$

$$Z_{EL} \cot \beta_{EL}(L_L - l) = Z_{DL} \tan \beta_{DL} l. \tag{14b}$$

These are rewritten in a more convenient form

$$\sqrt{\bar{\epsilon}_U} = \tan\left[\frac{\pi}{2}\sqrt{\bar{\epsilon}_U}\,\frac{l}{L_U}\,\frac{f_U}{f_{EU}}\right] \tan\left[\frac{\pi}{2}\left(1 - \frac{l}{L_U}\right)\frac{f_U}{f_{EU}}\right] \tag{15a}$$

$$\sqrt{\bar{\epsilon}_L} = \tan\left[\frac{\pi}{2}\sqrt{\bar{\epsilon}_L}\,\frac{l}{L_L}\,\frac{f_L}{f_{EL}}\right] \tan\left[\frac{\pi}{2}\left(1 - \frac{l}{L_L}\right)\frac{f_L}{f_{EL}}\right]. \tag{15b}$$

These equations are identical for lower and upper cutoff frequencies. They do not contain the characteristic impedances explicitly. They are solved in the following way.

$\sqrt{\bar{\epsilon}_U}$ or $\sqrt{\bar{\epsilon}_L}$ is considered a given parameter. Then the frequency ratio f_U/f_{EU} or f_L/f_{EL} is a function of l/L_L or l/L_U. This function requires the solution of transcendental equation (15a) or (15b). Numerical values were obtained by machine computations using the IBM 7090. The results are plotted in Fig. 8.

This graph can then be used to determine the upper and lower cutoff frequencies of the loaded comb structure. It is assumed here that the upper and lower cutoff frequencies of the empty comb, f_{EU} and f_{EL}, and connected with them, the effective finger lengths, L_U and L_L, are known. They are best determined by measurement, but they could also be calculated from the fringe capacity and the characteristic impedance. The quantity yet to be evaluated is the effective dielectric constant, $\bar{\epsilon}_U$ and $\bar{\epsilon}_L$, before the cutoff frequencies can be read from the graph in Fig. 8. It will be necessary, however, to work out the electric field pattern within the unloaded comb, then in the loaded section, including the respective characteristic impedances, before the effective dielectric constant can be obtained.

III. FIELD PATTERN AND CHARACTERISTIC IMPEDANCE OF UNLOADED COMB

3.1 *Upper Cutoff Frequency*

The electric field pattern of the unloaded one-finger model will look about like Fig. 9(a). This geometry is, unfortunately, too complicated for a closed analytical treatment. On the basis of the geometry and the mathematical tools at hand, the following approach may be suggested. The area available to the electric field is divided into four regions, two equivalent regions of type A and two equivalent regions of type B, as shown in Fig. 9(b). Two further approximations are then necessary.

(*v*) *The electric field in the regions A can be represented as a homogeneous, parallel plate condenser field.*

(*vi*) *The electric field in the regions B can be represented by the field produced by an infinitely thin metal fin inserted in a rectangular enclosure of corresponding dimensions.*

These approximations are illustrated in Figs. 9(c) and 9(d). Along the joints of regions A and B the field thus assumed is discontinuous. In reality, it is inhomogeneous near the boundary of region A, and it is less inhomogeneous than assumed near the boundary of region A because there is only a 90° bend, not a 180° bend as in the model used. These

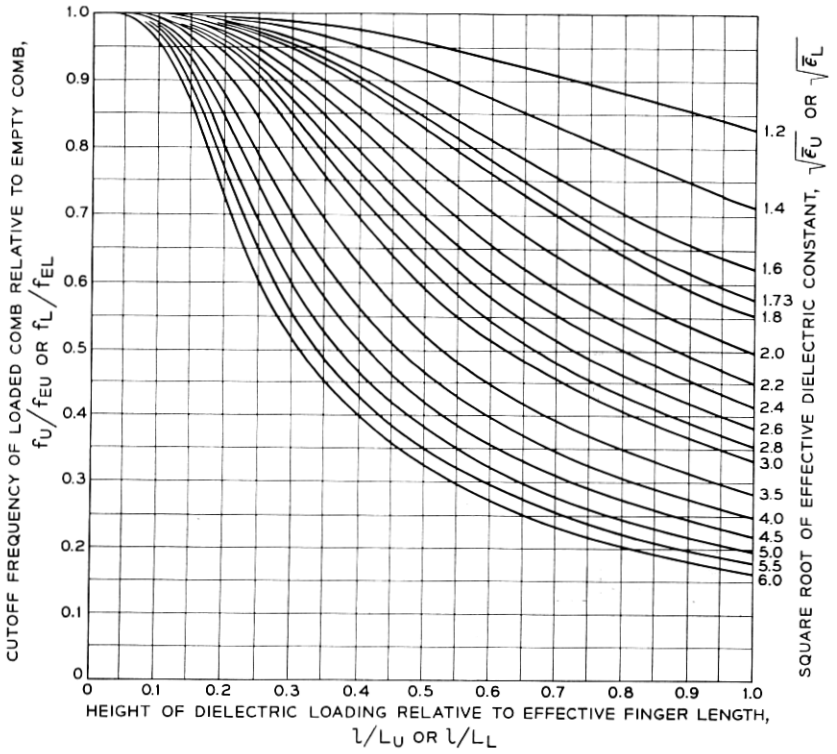

Fig. 8 — Plot of numerical values obtained by machine computations.

discrepancies of the field model from what would be expected should in reality be very small, particularly if the gap between finger and wall, the dimension $W_A = \frac{1}{2}(1 - r)D_U$ defined in Figs. 9(a) and 9(e), is small compared to other dimensions. This is so in cases of practical interest.

As far as the impedance is concerned, the two regions A and the two regions B are in parallel. The impedance of a region A is simply the ratio of its dimensions multiplied by free-space impedance. The impedance of region B is not as easily found. It is possible, however, to use a conformal transformation which maps the region B into a parallel plate geometry. This is schematically indicated in Fig. 9(e). The transformation actually utilized consists of the consecutive application of two transformations, each using elliptical functions. The procedure, including the mathematical details of the conformal transformation by elliptical functions, is outlined in the Appendix.

It is known from the theory of conformal mapping by functions of

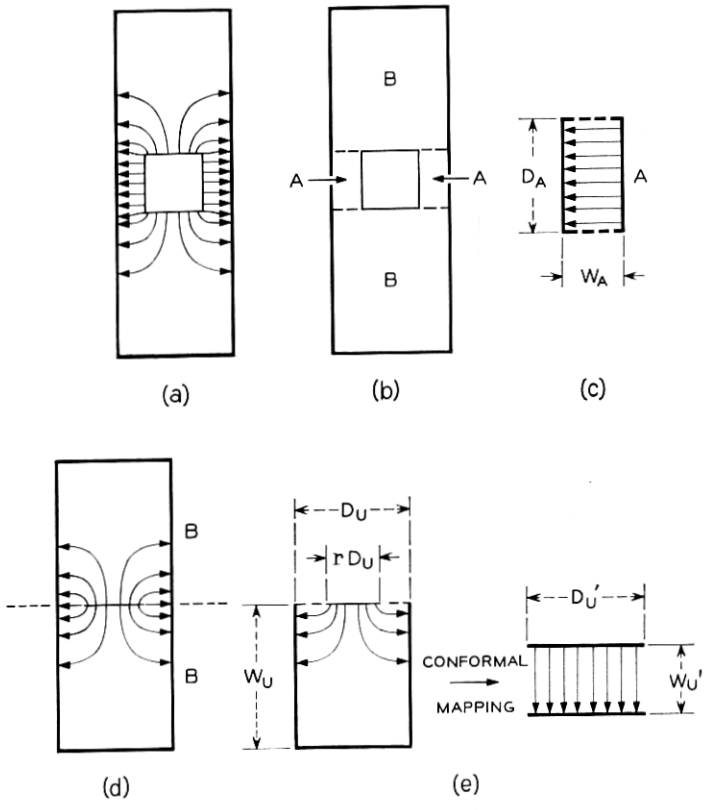

Fig. 9 — Analysis for upper cutoff frequency: (a) real field patterns, (b) regions used for analysis, (c) homogeneous field assumed in region A, (d) fin field assumed in region B, (e) fin field equivalent to homogeneous field.

complex variables that the geometry is preserved in infinitesimal regions. In particular, it is clear that infinitesimal squares with boundaries formed by field lines and equipotential lines continue to be squares. Since the impedance can be thought of as composed of the impedance of these infinitesimal squares, partly in parallel and partly in series as indicated by the over-all geometry, it follows finally that the impedance of the two transmission lines of Fig. 9(e) is the same.

The geometry before transformation is characterized by the two ratios: W_U/D_U and r. Thus W_U'/D_U' will be a function of both of these ratios. So far only combs with $r = \frac{1}{2}$ have been investigated in practice. For convenience, therefore, the subsequent calculations are carried out for this value of r. This implies a further restriction.

(vii) In the numerical calculations to follow, only comb geometries with the finger width as large as the gap between fingers are considered.

From a mathematical point of view, this restriction is somewhat arbitrary. Any other choice of r, the ratio of finger width to length of period, however, would necessitate another application of the elliptic integral conformal transformation.

With $r = \frac{1}{2}$, W_U'/D_U' is a single-valued function of W_U/D_U. This function is plotted in Fig. 10, An interesting feature of this graph is that W_U'/D_U' goes asymptotically to $\frac{1}{2}$; it reaches this value to within 2 per cent at $W_U/D_U = 0.65$. The physical interpretation of this observation is as follows. For $W_U/D_U > 0.65$, essentially all the field lines originating at the center fin in Fig. 9(d) terminate on the side wall; none reach the opposite end wall. Therefore, this wall can be moved out toward infinity with no noticeable effect on the impedance at the upper cutoff frequency.

The characteristic impedance of the empty structure at the upper cutoff frequency can now be given. It is

$$Z_{0U} = 377 \text{ ohms} \Big/ \left(2\frac{D_A}{W_A} + 2\frac{D_U'}{W_U'}\right). \tag{16a}$$

An important special case is one where, first, W_U/D_U is greater than 0.65 so that the asymptotic value $W_U'/D_U' = \frac{1}{2}$ applies and where, second, the fingers have a square cross section so that $W_A/D_A = \frac{1}{2}$. Then the characteristic impedance is simply

$$Z_{0U} = \tfrac{1}{8} \times 377 \text{ ohms} = 47.1 \text{ ohms}. \tag{16b}$$

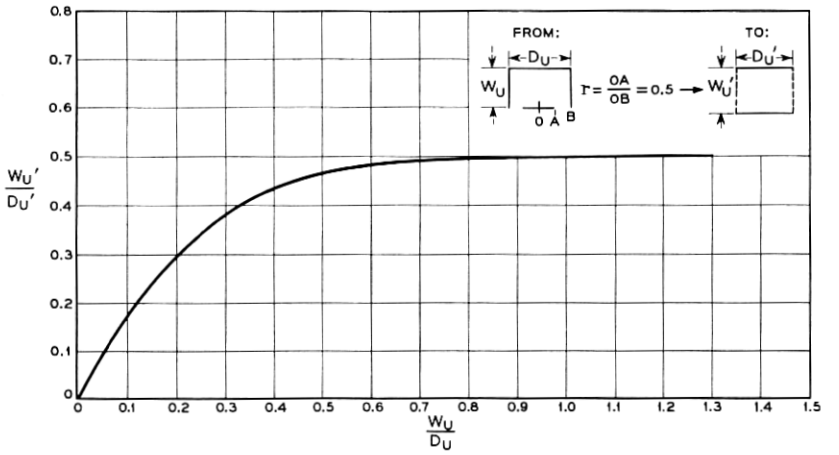

Fig. 10 — Conformal transformation for upper cutoff.

Since the partial impedances are equal, it also follows in this case that the total stored energy is equally distributed between the four regions A, A, B, B. This remark may be helpful in estimating the filling factor.

3.2 *Lower Cutoff Frequency*

The procedure here is quite similar to that in the case of the upper cutoff frequency. The field pattern is illustrated in Fig. 11(a). The cross-section area available to the electric field is divided into four regions, two electrically equivalent regions of type A and two regions of type B, as shown in Fig. 11(b). Again two approximations are required.

(*viii*) *The electric field in region A is so small that it can be neglected.*

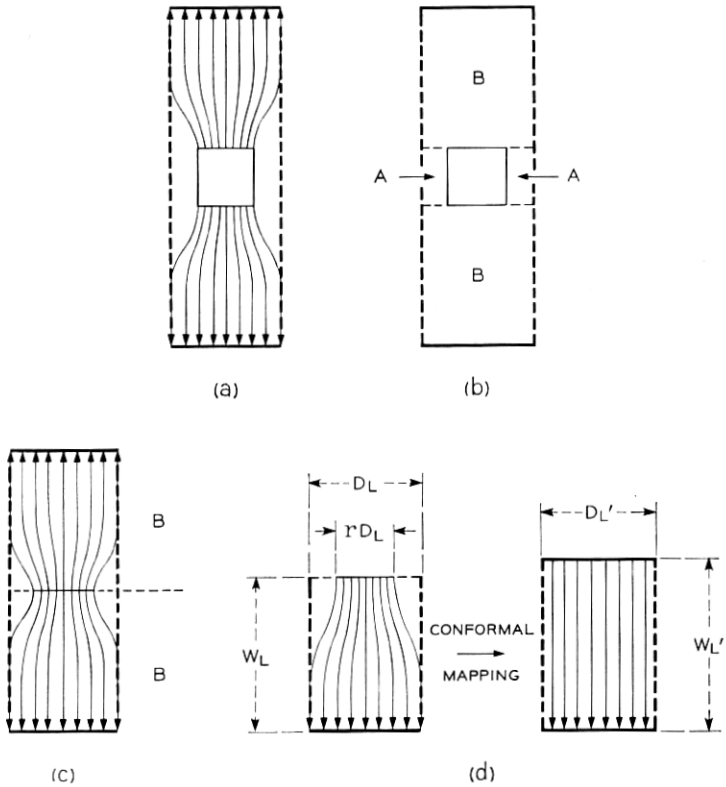

Fig. 11 — Analysis for lower cutoff frequency: (a) typical electric field pattern, (b) regions used for analysis, region A assumed field-free, (c) fin field assumed in region B, (d) fin field equivalent to homogeneous field.

(*ix*) *The electric field in region B can be represented by the field produced by an infinitely thin metal fin inserted into a rectangular enclosure with appropriate dimensions and boundary conditions.*

It is apparent that the approximation (*viii*) is justified. Only very small fringing fields will exist in region A. The implication of approximation (*ix*) is indicated in Fig. 11(c). It should also be very well justified, since there is no essential difference between the idealized field pattern and the real one. Region B can be transformed into a simple parallel plate geometry. This is indicated in Fig. 11(d). The transformation again consists of two consecutive conformal mappings by means of elliptic functions. The procedure is outlined in the Appendix. The impedance of region B is simply given by the aspect ratio W_L'/D_L' of the parallel plate geometry resulting from the transformation, multiplied by the free-space impedance. This resulting ratio W_L'/D_L' is a function of two ratios, r and W/D. For mathematical convenience and because of practical importance, only comb geometries with $r = \frac{1}{2}$ are considered in the subsequent calculations. For other ratios r, a new evaluation of the elliptical transformation is necessary. Thus restriction (*vii*) is invoked here, too.

(*vii*) *In the numerical calculations which follow, only comb geometries with the finger width equal to the gap width between fingers are considered.*

The single-valued function W_L'/D_L' of W_L/D_L with the parameter $r = \frac{1}{2}$ is shown in Fig. 12. The characteristic impedance of the empty structure at the lower cutoff frequency is then given by

$$Z_{0L} = \frac{W_L'}{2D_L'} \times 377 \text{ ohms.} \tag{17a}$$

As long as $W_L/D_L > 0.2$, it is seen from the graph that this can be approximated by

$$Z_{0L} = \frac{1}{2}\left(\frac{W_L}{D_L} + 0.11\right) 377 \text{ ohms.} \tag{17b}$$

The asymptotically linear curve in Fig. 12 and this last equation suggest an almost obvious interpretation. The electrical behavior of region B is essentially the same as that of a parallel plate geometry having the same width $D_L' = D_L$, but a slightly greater distance between plates, $W_L' > W_L$. Also, the asymptotic slope for the curve is unity. Considering a geometry with $W_L/D_L > 0.2$, this would mean the following. If W_L is increased further, the electric field pattern near the fin stays the same, while the added volume away from the finger is taken up by a homogeneous electric field.

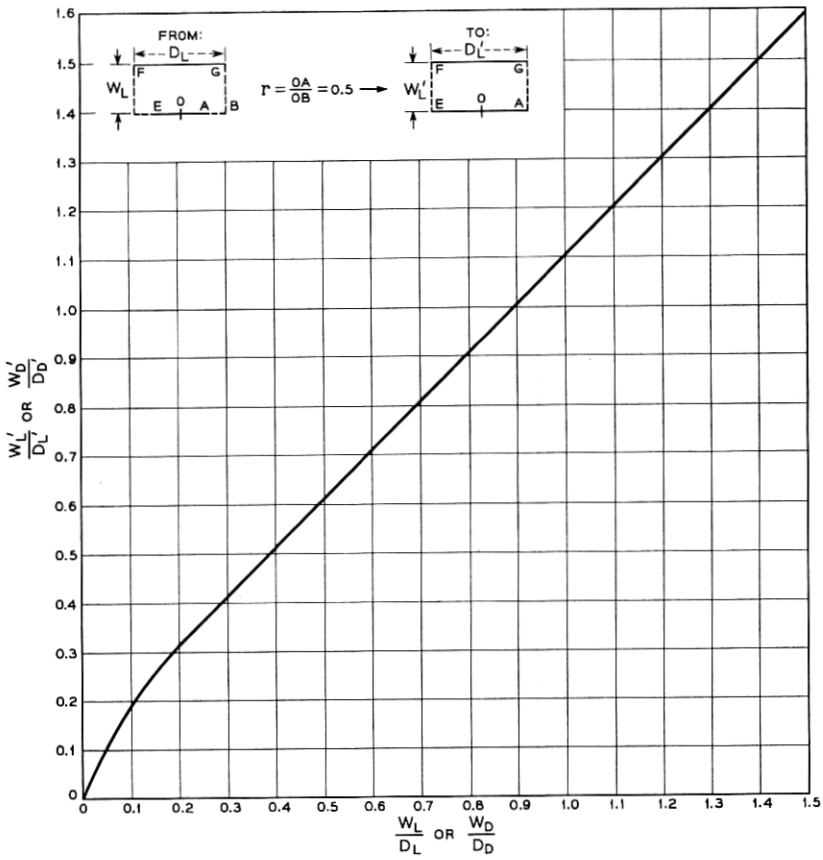

Fig. 12 — Conformal transformation for lower cutoff.

IV. CAPACITANCE AND EFFECTIVE DIELECTRIC CONSTANT OF COMB PARTIALLY FILLED WITH DIELECTRIC

It was mentioned that the electromagnetic field configuration in the comb line partially loaded with dielectric should be treated as a TEM mode. It was pointed out that this is equivalent to finding a static solution of the electric field problem. Thus the problem here is to find the static value of the capacitance per unit length of the loaded finger line. The difference in electrical behavior of the loaded line compared to the unloaded line is then fully expressed by an effective dielectric constant. This effective dielectric constant is simply the ratio of the static capacitance of the loaded line to the capacitance of the unloaded line.

4.1 *Upper Cutoff Frequency*

The field pattern in the presence of one dielectric slab is illustrated in Fig. 13. It is seen that the dielectric is present in one of the regions called B before. The usual boundary conditions for the continuity of the tangential E vector and of the normal D vector have to be observed in fitting together the electric field pattern inside and outside the dielectric.

At first sight it seems that no difficulty is incurred in this respect at the boundary of the dielectric. In the model chosen for the field configuration, the field lines run parallel to the boundary both in regions A and B. The boundary condition for tangential electric field seems to apply, with the consequence that the field pattern remains the same in the dielectric as before in the unloaded region B. Calculations are based on this assumption, and they are presumably of sufficient accuracy for present purposes.

There is a small error in this assumption. It was pointed out before that the two models chosen to represent the field in regions A and B do not match at the boundary. In the models, the field in A is homogeneous, that in B strongly inhomogeneous. The real field at the boundary of A and B should be somewhere between these two extremes. It is expected,

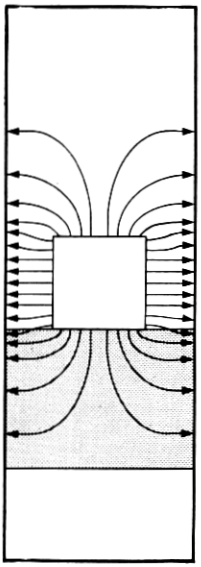

Fig. 13 — Electric field pattern at upper cutoff with dielectric loading present.

therefore, that the error in the impedance calculation of the empty comb at the upper cutoff frequency is negligible. The same is not necessarily true in the presence of dielectric. The real, inhomogeneous field in the region near the boundary of A and B will be disturbed by the insertion of dielectric. The deviations of the real field from that used in the calculations — homogeneous in A, elliptic function field in B — are now accentuated by a high dielectric constant rather than evened out as in the empty comb. This will lead to an error in the calculation of the capacitance and the effective dielectric constant. Hence it is not trivial that the approximations (*v*) and (*vi*) are still reasonably good in the presence of dielectric. Fortunately, it can be argued that the error incurred by this approximation is still negligible within the accuracy sought for here and with respect to typical structure geometries and dielectric constants considered. A formulation of the approximation follows.

(*x*) *In the presence of dielectric loading, the static electric field can still be represented by a homogeneous, parallel plate field in region A and the field of a metal fin inside a rectangular enclosure in region B filled by the dielectric.*

The next concern is the other boundary of the dielectric away from the finger. Here the field lines cross the boundary at all directions between tangential and perpendicular. It would be very difficult to apply boundary conditions to this field pattern. Therefore another restriction is introduced.

(*xi*) *The calculation is restricted to dielectric loadings thick enough so that essentially the total electric field energy of region B is contained within the dielectric.*

The numerical implication of this restriction follows directly from Fig. 10. It is assumed that the fingers are as wide as the gap between them. From the graph the following fact can be deduced. If a geometry is considered where W_U is considerably larger than D_U, then 98 per cent of the electric field energy is concentrated in a rectangle near the finger, D_U wide and 0.65 D_U deep. Restriction (*xi*) thus implies that only dielectric slabs which have a thickness of at least 0.65 times the length of a period of the comb are considered.

Fortunately, this restriction does not exclude any cases of practical interest. Since the field configuration on the finger is treated here as a TEM mode, the filling factor in the plane perpendicular to the finger is the same for the dielectric and the magnetic field energy. Thus, slabs thinner than indicated by restriction (*xi*) would also have a reduced gain interaction near the upper cutoff frequency, since not all of the magnetic field energy of region B would be contained in the maser material. Gain

is still at a premium in present TWM development, and thus it does not seem to be necessary to treat cases other than those restricted by (*xi*).

It is now possible to write down the capacitance and the effective dielectric constant. By comparison with (16a), it is seen that the capacitance per unit length of the empty one-finger line is

$$c_{EU} = \epsilon_0 \left[2 \frac{D_A}{W_A} + 2 \frac{D_U'}{W_U'} \right]. \tag{18}$$

(Lower case c is used to distinguish this quantity from the fringe capacity C_U.) With dielectric loading on one side of the finger

$$c_{DU} = \epsilon_0 \left[2 \frac{D_A}{W_A} + (\epsilon + 1) \frac{D_U'}{W_U'} \right] \cdots . \tag{19a}$$

Similarly, if the dielectric is loaded on both sides of the finger

$$c_{DU} = \epsilon_0 \left[2 \frac{D_A}{W_A} + 2\epsilon \frac{D_U'}{W_U'} \right] \cdots . \tag{19b}$$

The effective dielectric constant is then simply, for loading on one side

$$\bar{\epsilon}_U = [(\epsilon + 1) + 2b]/[2 + 2b] \tag{20a}$$

and for loading on both sides

$$\bar{\epsilon}_U = (\epsilon + b)/(1 + b) \tag{20b}$$

with

$$b = D_A W_U'/W_A D_U'. \tag{21}$$

Most important perhaps for present applications is the case where, first, the fingers are square so that (16b) applies and where, second, the dielectric is ruby with an isotropic average dielectric constant of $\epsilon = 9$. In that case, for loading on one side

$$\bar{\epsilon}_U = 3 \tag{22a}$$

and for loading on both sides

$$\bar{\epsilon}_U = 5. \tag{22b}$$

4.2 *Lower Cutoff Frequency*

The field pattern in the presence of one dielectric slab is illustrated in Fig. 14. The dielectric fills part of the region called B before. For the evaluation of the capacitance it is significant that restriction (*xi*) is applied here, too. Then the following approximation can be made.

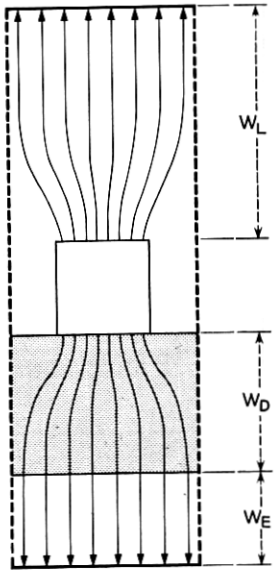

Fig. 14 — Electric field pattern at lower cutoff with dielectric loading present.

(*xii*) *In the presence of dielectric loading, the static electric field can be represented in the following way: There is zero field in region A; in the dielectric there is a field like that produced by a metal fin in a rectangular enclosure, having the dimensions of the dielectric and subject to appropriate boundary conditions. The field past the dielectric is a homogeneous parallel plate field.*

It can be argued that these approximations are well justified. There is no potential difference between fingers; hence region A should be field-free except perhaps for some very small fringe fields. In connection with 17(b) it was shown that the field has its inhomogeneities near the finger, whereas the field region near the wall is reasonably homogeneous.

The capacitance per unit length of the loaded one-finger model can now be given. For the empty line it is

$$c_{EL} = 2\epsilon_0(D_L'/W_L'). \tag{23}$$

For the loaded line, the capacitance is obtained from two contributions in parallel, one from each side of the finger. The capacitance of the loaded side comes from two contributions in series: one from the dielectric, involving an elliptical transformation using the dimensions of the dielectric, and one a parallel plate contribution from the space behind the dielectric. Thus, for dielectric loading on one side

$$c_{DL} = \epsilon_0 \left[\frac{D_L'}{W_L'} + \left(\frac{W_D'}{\epsilon D_D'} + \frac{W_E}{D_E} \right)^{-1} \right] \tag{24a}$$

and for loading on both sides

$$c_{DL} = 2\epsilon_0 \Big/ \left(\frac{W_D'}{\epsilon D_D'} + \frac{W_E}{D_E} \right). \tag{24b}$$

Here W_D and D_D are the physical dimensions of the dielectric cross section per one-finger line, W_E and D_E the dimensions of the empty space behind the dielectric. W_D'/D_D' is obtained from W_D/D_D by means of the elliptical transformation illustrated in Fig. 11.

The effective dielectric constant can now be evaluated as the ratio c_{DL}/c_{EL}. The formulas, however, turn out to be fairly long. They are given here, therefore, only for the case that the approximation in (17b) is valid both for the empty structure and the dielectric. It is further observed that

$$D_L = D_D = D_E = D$$

and

$$W_L = W_D + W_E .$$

Then the effective dielectric constant for dielectric loading on one side is

$$\bar{\epsilon}_L = \tfrac{1}{2} \frac{2\epsilon W_L - (\epsilon - 1)W_D + (\epsilon + 1)0.11D}{\epsilon W_L - (\epsilon - 1)W_D + 0.11D} \tag{25a}$$

and similarly, for loading on both sides

$$\bar{\epsilon}_L = \epsilon \frac{W_L + 0.11D}{\epsilon W_L - (\epsilon - 1)W_D + 0.11D} . \tag{25b}$$

It is seen that the effective dielectric constant is a function of ϵ, W_D/W_L and D/W_L. Once a particular structure geometry has been picked, then D/W_L is known. If a particular maser material is selected, ϵ is known. Then $\bar{\epsilon}_L$ is a unique function of the relative loading thickness, W_D/W_L. One example of such a function is given in Fig. 15. For convenience in using the graph of Fig. 8, the square root $\sqrt{\bar{\epsilon}_L}$ is given instead of $\bar{\epsilon}_L$. Curves for effective constants based on other parameters can easily be calculated using either (25a) or (25b).

V. EXAMPLE FOR DESIGN PROCEDURE

In Sections III and IV the empty and the dielectrically loaded comb structure were evaluated. Field pattern, impedance and propagation constants were obtained for both the upper and lower cutoff frequencies.

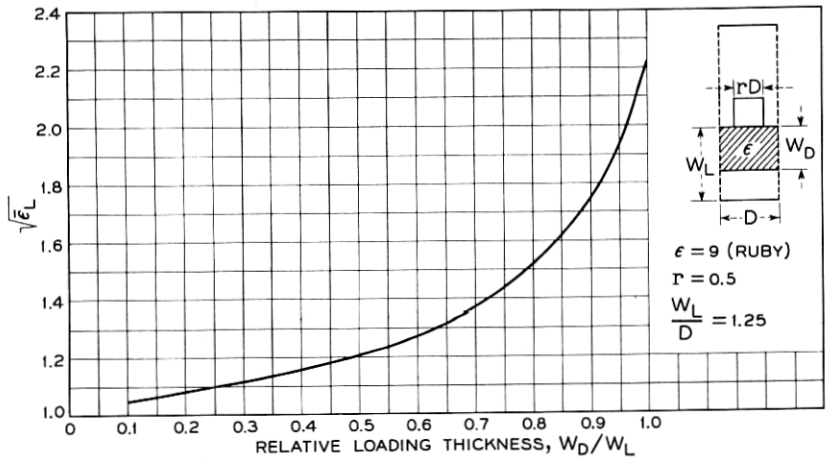

Fig. 15 — $\sqrt{\epsilon_L}$ vs relative loading thickness, one side only, loaded at lower cutoff frequency for parameters indicated.

With this information at hand, it is now possible to arrive at a numerical design procedure. The aim is to predict the cross-sectional dimensions of a dielectric parallelepiped which will simultaneously tune the upper and lower cutoff frequencies of the comb structure to some predetermined values. Of course, it is not possible to ask for completely arbitrary design cutoff frequencies. Obviously there are limits to the amount of tuning which can be achieved by a given dielectric material within a given comb geometry. These limits can also be determined easily by the analysis.

The design procedure follows the outlines given briefly at the end of Section II. It can now be described in general terms. Perhaps it is advantageous, however, to illustrate the procedure by means of an example. The example to be described is a case of a "design on paper." That is to say, the design calculations can be made entirely on the basis of calculable values. It is not necessary to fabricate a size or scale model of the comb structure under consideration in order to determine certain values by measurement. The only empirical value required is the fringe capacity between finger tip and the structure enclosure; this may be obtained from Fig. 7.

One interesting and valuable feature of the design procedure is that of independently setting the upper and lower cutoff frequencies. This is possible because the upper cutoff frequency can be controlled by adjusting the height l of the dielectric loading alone, and because it is not dependent in any way on the dielectric thickness W_D as long as W_D ex-

ceeds a certain small minimum value. Then the dimension W_D can be used to control the lower cutoff frequency independently.

As an example for the design procedure, a comb structure is considered with the following dimensions:

(a) finger length 0.400 inch
(b) spacing between fingers 0.040 inch
(c) finger cross section 0.040 square inch
(d) wall-to-wall spacing of enclosure 0.240 inch.

As further information, the fringe capacity was measured in an electrolytic tank model and was found to be (see Fig. 7 for gap spacing greater than 70 mils):

(e) fringe capacity $C_L = 0.025\ \mu\mu F$, $C_U = 0.035\ \mu\mu F$.

The problem considered is that of finding the dimensions for a single ruby parallelepiped which brings the upper cutoff frequency to 4200 mc and the lower cutoff frequency to 3210 mc.

First step: Find effective finger length at the upper cutoff frequency of the empty comb.

Equation (10a) applies for the increase in length and (16b) applies for the impedance; thus

$$\begin{aligned}\Delta l_U &= Z_{EU} C_U c \\ &= 47.1 \times 0.025 \times 10^{-12} \times 3 \times 10^{10} \\ &= 0.035 \text{ cm}.\end{aligned}$$

The effective length for upper cutoff is then [see (8a)]

$$\begin{aligned}L_U &= L' + \Delta l_U \\ &= 2.54 \times 0.400 + 0.035 = 1.051 \text{ cm}.\end{aligned}$$

This corresponds to an upper cutoff frequency for the empty comb [see (8a)]

$$\begin{aligned}f_{EU} &= c/4L_U \\ &= 7150 \text{ mc}.\end{aligned}$$

Thus the design specification

$$f_U = 4200 \text{ mc}$$

is equivalent to specifying a ratio of

$$f_U/f_{EU} = 0.587.$$

Second step: Find in an analogous way the effective finger length at the lower cutoff frequency of the empty comb.

Equation (17b) applies for the impedance. From the dimensions given, $W_L = 0.100''$, $D_L = 0.080''$, hence

$$Z_{EL} = \frac{1}{2}\left(\frac{W_L}{D_L} + 0.11\right) 377 \text{ ohms}$$
$$= 256 \text{ ohms}.$$

The addition to length is given by (10b)

$$\Delta l_L = Z_{EL} C_L c$$
$$= 256 \times 0.035 \times 10^{-12} \times 3 \times 10^{10}$$
$$= 0.268 \text{ cm}.$$

The effective length for lower cutoff becomes

$$L_L = L' + \Delta l_L$$
$$= 0.400 \times 2.54 + 0.268$$
$$= 1.284 \text{ cm}$$

corresponding to a cutoff frequency for the empty comb

$$f_{EL} = c/4L_L$$
$$= 5840 \text{ mc}.$$

The design specification of

$$f_L = 3210 \text{ mc}$$

is thus equivalent to specifying a ratio

$$f_L/f_{EL} = 0.55.$$

Third step: Satisfy the upper cutoff frequency specification by choosing an appropriate dielectric height l without regard for W_D, the thickness of the loading. This is possible because, as mentioned before, the effective dielectric constant at the upper cutoff frequency is independent of loading thickness. The effective dielectric constant, $\bar{\epsilon}_U$, for one-sided loading with ruby is 3 from (22a); thus

$$\sqrt{\bar{\epsilon}_U} = 1.73.$$

Consulting Fig. 8 for the dielectric height which makes $f_U/f_{EU} = 0.59$ with the parameter $\sqrt{\bar{\epsilon}_U}$, it is seen that

$$l/L_U = 0.96.$$

Hence, the dielectric loading height should be

$$l = 0.96 \times 1.051 = 1.010 \text{ cm}$$
$$= 0.398''$$

In other words, the dielectric loading height turns out to be very nearly the same as the finger length.

Fourth step: Satisfy the lower cutoff frequency specification by choosing an appropriate thickness W_D of the dielectric loading. This is done by the following successive measures.

From the loading height l just determined find

$$l/L_L = 1.010/1.284$$
$$= 0.79.$$

Enter the graph of Fig. 8 with $l/L_L = 0.79$ and $f_L/f_{EL} = 0.55$. The value interpolated at the point having these two coordinates is

$$\sqrt{\bar{\epsilon}_L} = 2.22.$$

The graph of Fig. 15 is valid for present calculations; entering this last value into the graph it is found that

$$W_D = W_L$$

hence

$$W_D = 0.100 \text{ inch.}$$

The final answer, then, is that the comb described initially will have the specified cutoff frequencies if a slab of ruby of height 0.398 inch and of width 0.100 inch is inserted.

An experiment was carried out to check the results of this calculation. The two cutoff frequencies of a comb as specified above were measured after inserting a single slab of polycrystalline high density alumina (dielectric constant $\approx$9.3) with cross-sectional dimensions of 0.400 inch and 0.100 inch. The cutoff frequencies measured were 4200 mc and 3210 mc respectively. These frequencies were then specified as design frequencies for the above example. The close agreement between the actual dimensions of the alumina slab and those calculated by the present recipe is gratifying. It may be argued, however, that the obtained agreement is somewhat fortuitous. In particular, one should expect that the fringe capacity is altered if the dielectric loading extends all the way along the fingers up to the finger tips. To investigate the accuracy of the present analysis, a series of systematic measurements was made.

For this study a number of short sections of comb structures were built and tested. They all had finger dimensions of 0.040 × 0.040 × 0.445 inch, and the fingers were spaced 0.080 inch on center. The structures were loaded symmetrically with two slabs of high-density polycrystalline alumina (dielectric constant quoted to be 9.3) of full finger height. The geometry and the result of the measurements are shown in Fig. 16. In two series of measurements, the fraction of the housing width filled by the alumina loading, W_D/W_L, was held at 0.90 and 0.95, respectively, while the gap width between the finger and the housing wall, $W_L = W_U$, was varied in the range $0.75D$ = 0.060 inch, D = 0.080 inch, $1.25D$ = 0.100 inch and $1.5D$ = 0.120 inch. From the analysis, it is known that f_U should be independent of these dimensional changes. This is borne out by the experiment. Both the experimental points and the solid line for the theoretical value of f_U show the frequency independence. It is observed, however, that the experimental frequencies are 3.5 per cent higher. A somewhat greater disagreement is found for the lower cutoff frequency, which seems to indicate a systematic trend between theory and experiment. It can be said, however, that the largest deviations are

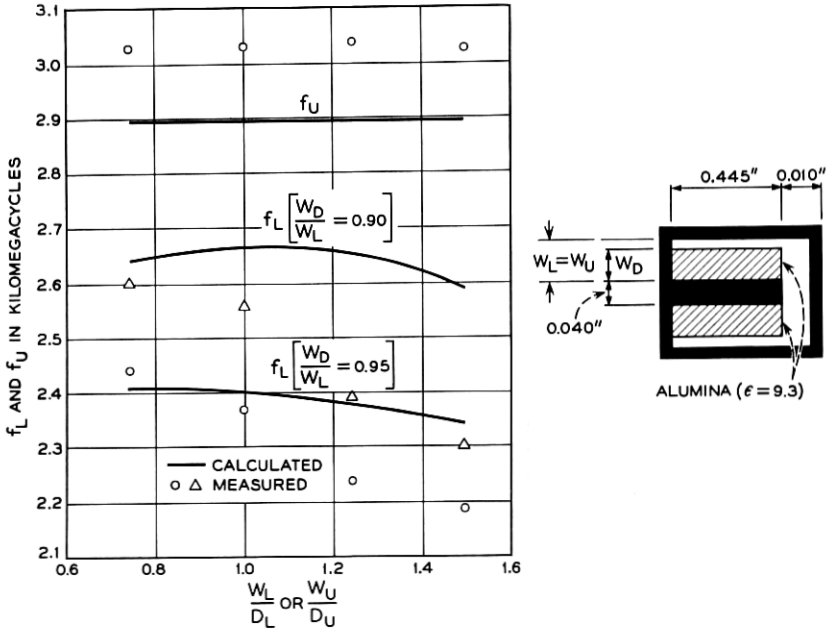

Fig. 16 — Examples of measured and calculated cutoff frequencies; the insert shows the comb geometry used.

10 per cent and that the typical discrepancy between theory and experiment is less than 5 per cent. The chance for greater systematic errors increases, of course, if comb and loading geometries are considered which comply less rigorously with the restrictions and approximations made in the text.

The numerical examples shown demonstrate that dielectric loading indeed decreases the fundamental passband frequency of the empty comb by a very appreciable factor. A one-sided loading with ruby may reduce the frequencies by a factor of 1.7, while double-sided loading may lead to a reduction by a factor 2.5. Still greater reductions may be obtained by using dielectric materials with higher dielectric constants and by modified comb geometries, in particular by changing the finger cross section from square to rectangular. It is also clear from this treatment that the shaping of the dielectric loading can be used to vary the degree of slowing within wide limits. These remarks may suffice here to illustrate the prominent role of dielectric loading techniques in the field of TWM development which was pointed out in the Introduction.

Since the original derivation of this analysis in 1960,[4] several TWM's have been developed in this laboratory. They include the TWM for the ground station receiver in the Telstar satellite communication experiment[6] and radio astronomy TWM preamplifiers for hydrogen line work at 1420 mc.[7] In these cases, the analysis has proved to be a valuable aid for arriving at a first-order design and similarly for providing guidelines in the subsequent improvements of these designs.

APPENDIX

The conformal mapping transformations are derived and evaluated, leading to the impedance transformation curves in Figs. 10 and 12. The mathematical treatment given here is not too extensive, because the type of transformation used is known from other areas of electrical engineering. Yet the description of the mathematical procedure is made reasonably complete so that it may be useful as a guide for treating other related problems: for example, traveling-wave masers where the finger width is not identical to the spacing between fingers.

A.1 *The Schwartz-Christoffel Transformation*

The particular conformal transformation used here is a special case of the more general Schwartz-Christoffel transformation. The theorem proved independently by these two mathematicians states that it is possible to find an analytical function which maps the inside of a polygon on the

complex plane into the upper half of this plane. The boundary of the polygon thus is mapped into the real axis. If two transformations are considered, one of the type mentioned, the other performing the inverse function, it follows that the inside of a polygon can be mapped into the inside of any other polygon.

The general Schwartz-Christoffel transformation is illustrated in Fig. 17. For purposes of discussion, it is perhaps easier to consider first the inverse transformation of the upper half of the complex plane into a polygon. The transformation will be accomplished by a function whose derivative is given by a product of the type

$$\frac{dz}{dw} = (w - a)^{(\alpha/\pi-1)}(w - b)^{(\beta/\pi-1)}(w - c)^{(\gamma/\pi-1)} \cdots. \qquad (26)$$

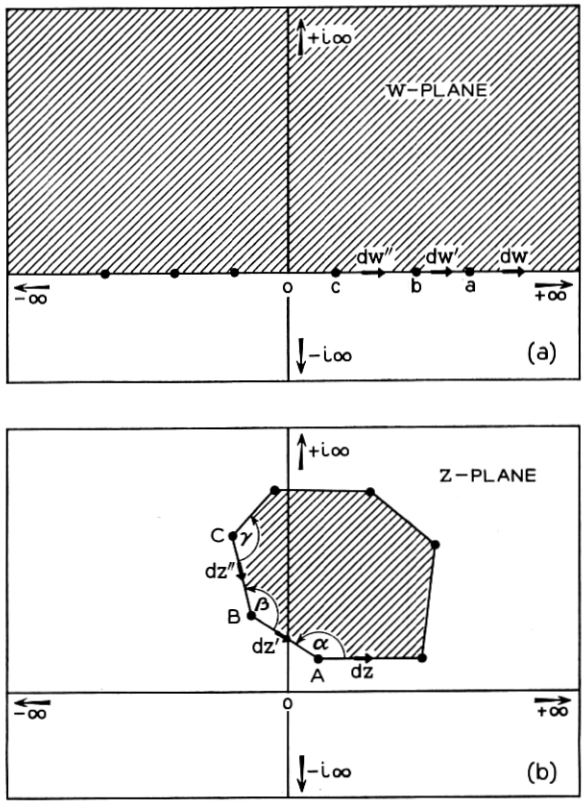

Fig. 17 — Illustration of the general mapping properties of the Schwartz-Christoffel transformation.

To demonstrate the transformation property, consider values of w and dw on the real axis. Also represent each factor in the form $r_k e^{i\phi_k}$ with a real number r_k for the magnitude and ϕ_k for the angle. It is seen then that for values w such that $w > a,b,c \cdots$ all the ϕ_k on the right-hand side of (26) vanish. Hence the angles of dz and dw are identical; that is, these line elements are parallel. Mathematically

$$\Delta dz = 0 \qquad \text{if } w \text{ and } dw \text{ are real and } w > a,b,c \cdots. \tag{27a}$$

For values $a < w < b$ the first bracket changes sign; that is, its angle is π. The angle of the first factor becomes $\alpha - \pi$

$$\Delta dz' = \alpha - \pi \qquad \text{if } w \text{ and } dw' \text{ are real and } a > w > b,c \cdots. \tag{27b}$$

That is to say, the real axis of the w plane near a is transformed in the z plane into a polygon corner at some as yet undetermined point A including an angle α. Similarly

$$\Delta dz'' = \alpha + \beta - 2\pi \qquad \text{if } w \text{ and } dw'' \text{ are real and } a,b > w > c \cdots \tag{27c}$$

indicating another polygon corner at B including an angle β and corresponding to the point b on the real axis of the w plane.

In this fashion, it is shown that the transformation (26) indeed maps the upper half of the w plane into the inside of a polygon having specified angles $\alpha, \beta, \gamma \cdots$ at points in the z plane corresponding to $a,b,c \cdots$ in the w plane. While it is thus easy to satisfy conditions on the angles of the polygon, the difficulty is to find the points $A,B,C \cdots$ in the z plane which correspond to $a,b,c \cdots$ in the w plane. This requires an evaluation of the integral of (26).

Even more typical for engineering applications, and important in the present example, is the inverse situation. The corner points $A,B,C \cdots$ of the polygon are given. Then the problem is to find the real numbers $a,b,c \cdots$ which when inserted into (26) will transform this polygon into the upper half of the w plane. In most cases, this problem can only be solved numerically. The procedure would be to tabulate integrals of (26) for some range of values $a,b,c \cdots$. Numbering such tables with the given integral values $A,B,C \cdots$, the appropriate transformation parameters a,b,c could be picked.

To keep the need for tabulation down to a manageable chore, the number of significant parameters has to be restricted as much as possible. The example of importance in this connection is the mapping of a rectangle into the upper half of the complex plane. The number of significant parameters here can be reduced to one, the length ratio of two adjacent sides. Other parameters can be eliminated by trivial transformations

such as scaling and rotation of the coordinate system, which is accomplished simultaneously by a complex constant factor in (26) or a shift of the coordinate origin which corresponds to the integration constant of (26).

A.2 *Mapping of a Rectangle into the Upper Half of the Complex Plane*

It is now possible to write down the transformation equation for a rectangle. The conventional notation is illustrated in Fig. 18. The corners of the rectangle in the z plane are the complex numbers K, $K + iK'$, $-K + iK'$ and $-K$. In the w plane they correspond to the points 1, $1/k$, $-1/k$ and -1 on the real axis.

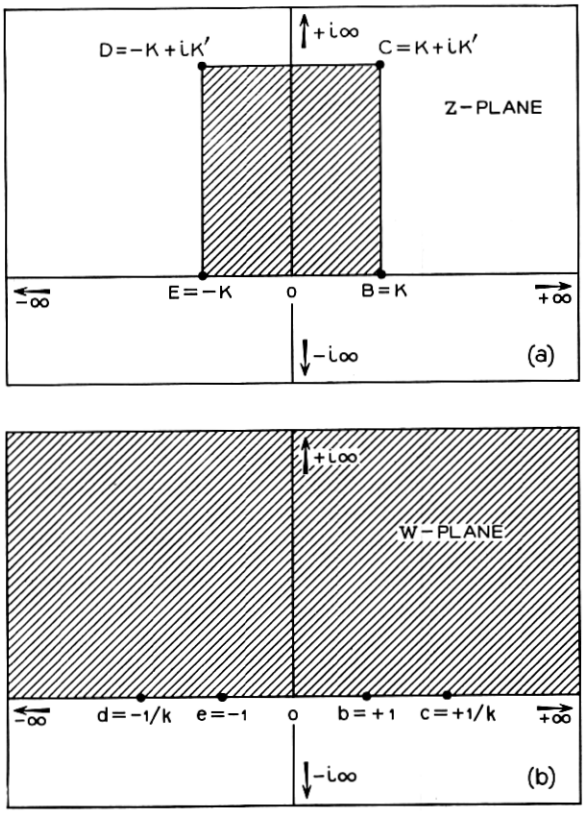

Fig. 18 — Illustration of the transformation of a rectangle in the z plane into the upper half of the w plane, introducing the conventional mathematical notation.

From (26) the transformation derivative is

$$\frac{dz}{dw} = A\left(w - \frac{1}{k}\right)^{-\frac{1}{2}}(w-1)^{-\frac{1}{2}}(w+1)^{-\frac{1}{2}}\left(w + \frac{1}{k}\right)^{-\frac{1}{2}}. \tag{28}$$

When the constant A is chosen appropriately ($A = -1/k$) this becomes

$$dz = \frac{dw}{(1-w^2)^{\frac{1}{2}}(1-k^2w^2)^{\frac{1}{2}}} \tag{29}$$

and

$$z = \int_{\omega=0}^{w} \frac{d\omega}{(1-\omega^2)^{\frac{1}{2}}(1-k^1\omega^2)^{\frac{1}{2}}}. \tag{30}$$

This integral is an elliptical integral of the first kind. It gives z as a function of w and k, where k is referred to as the modulus of the integral.

From the definition adapted in the figures it follows that

$$K = \int_{\omega=0}^{1} \frac{d\omega}{(1-\omega^2)^{\frac{1}{2}}(1-k^2\omega^2)^{\frac{1}{2}}} \tag{31}$$

and

$$iK' = \int_{\omega=1}^{1/4} \frac{d\omega}{(1-\omega^2)^{\frac{1}{2}}(1-k^2\omega^2)^{\frac{1}{2}}}. \tag{32}$$

K is called the complete elliptical integral. K' is the complete integral to the complementary modulus obeying the functional relationship

$$K'(k) = K(k') \tag{33}$$

where $k^2 + k'^2 = 1$ is used to define the modulus k' as complementary to k.

The definition of the elliptical integral of the first kind as given in in (30) is due to Jacobi. Many tables use also the notation of Legendre. This is obtained by setting

$$\begin{aligned} w &= \sin\phi, \qquad dw = \cos\phi\, d\phi \\ k &= \sin\theta, \qquad k' = \cos\theta. \end{aligned} \tag{34}$$

Then

$$z = \int_{\Psi=0}^{\phi} \frac{d\Psi}{(1-\sin^2\theta\sin^2\Psi)^{\frac{1}{2}}} \tag{35}$$

$$K = \int_{\Psi=0}^{\pi/2} \frac{d\Psi}{(1-\sin^2\theta\sin^2\Psi)^{\frac{1}{2}}} \tag{36}$$

$$K' = \int_{\Psi=0}^{\pi/2} \frac{d\Psi}{(1-\cos^2\theta\sin^2\Psi)^{\frac{1}{2}}}. \tag{37}$$

From this discussion it is clear that the transformation of a rectangle into the upper half plane requires finding the modulus k or equivalently the modular angle θ of the elliptical integral *from the given geometry of the rectangle*. It is further clear that K and K' are not independent, but related through either (31) and (32) or (36) and (37). Therefore, it is not possible to specify both length dimensions of the rectangle of Fig. 18 but rather only their ratio. The problem thus is reduced to finding the dependence of the modulus k or θ from the aspect ratio $K'/2K$ of the rectangle.

This functional dependence was evaluated using the Smithsonian Elliptic Function Tables, in particular tables of complete elliptical integrals. The result is presented in Fig. 19.

It should be added that frequently, instead of the elliptical integral (30), its inverse is used. This inverse function is written

$$w = \text{sn } z \text{ modulo } k \tag{38}$$

which is defined to mean (30). This notation is reminiscent of the sine function, with which the sn function is indeed identical in the special case $k = 0$.

A.3 *Mapping of the Upper Cutoff Frequency Configuration*

It is now possible to carry out the mapping transformations used in the comb structure analysis. The initial geometry for the lower cutoff frequency is indicated in Fig. 20(a), where solid lines represent conducting electrodes. The final result is a parallel plate geometry like that of Fig. 20(d). This figure represents the cross section of an idealized transmission line for which the impedance is simply given by the ratio of the length dimensions times free-space impedance. The transformation makes use of two intermediate steps. The interior of the rectangle (Fig. 20a) is first mapped into the upper half of the complex plane (Fig. 20b). Then a readjustment of the scale leads to Fig. 20(c). Then the upper half plane is finally mapped into the inside of the desired rectangle (Fig. 20d) with electrodes only on opposite sides.

To keep track of these steps, the relevant points in the original geometry and their transforms are denoted by capital letters O,A,B $\cdots$. The first and second elliptical transformations are distinguished by indices 1 and 2 attached to the modulus and the complete integral values. The mapping then proceeds as follows.

(*a*) *From the z plane to the y plane.*

$$y = \text{sn } z \text{ modulo } k_1 = \sin \theta_1 \tag{39}$$

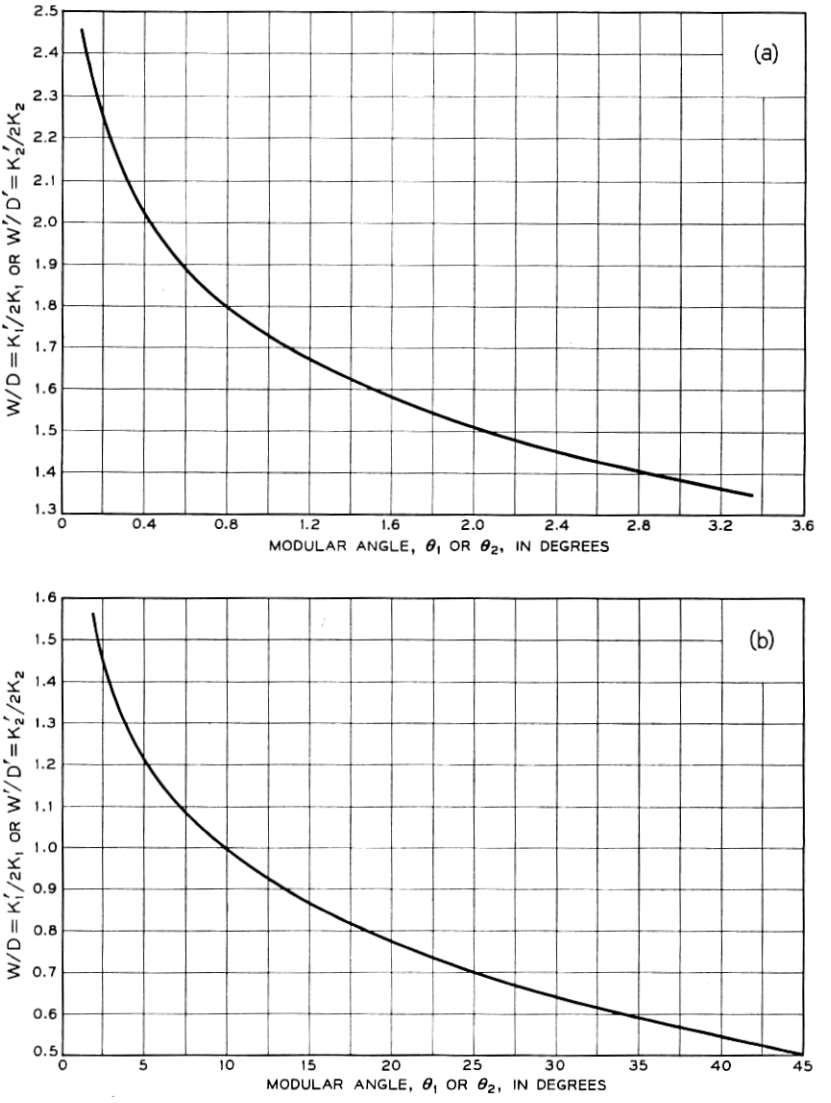

Fig. 19 — Relation between the ratio of the length dimensions of the rectangle to be transformed and the modular angle of the transforming elliptical function.

The modular angle θ_1 is found by entering the curves of Fig. 19 with the aspect ratio $W/D = K_r'/2K_1$ of the original rectangle. The corresponding coordinates in the z and y planes are given in Table I. The transformation of points O through D requires only the graph of Fig. 19. For points A and F, use has to be made of elliptic function tables. In the Smithsonian

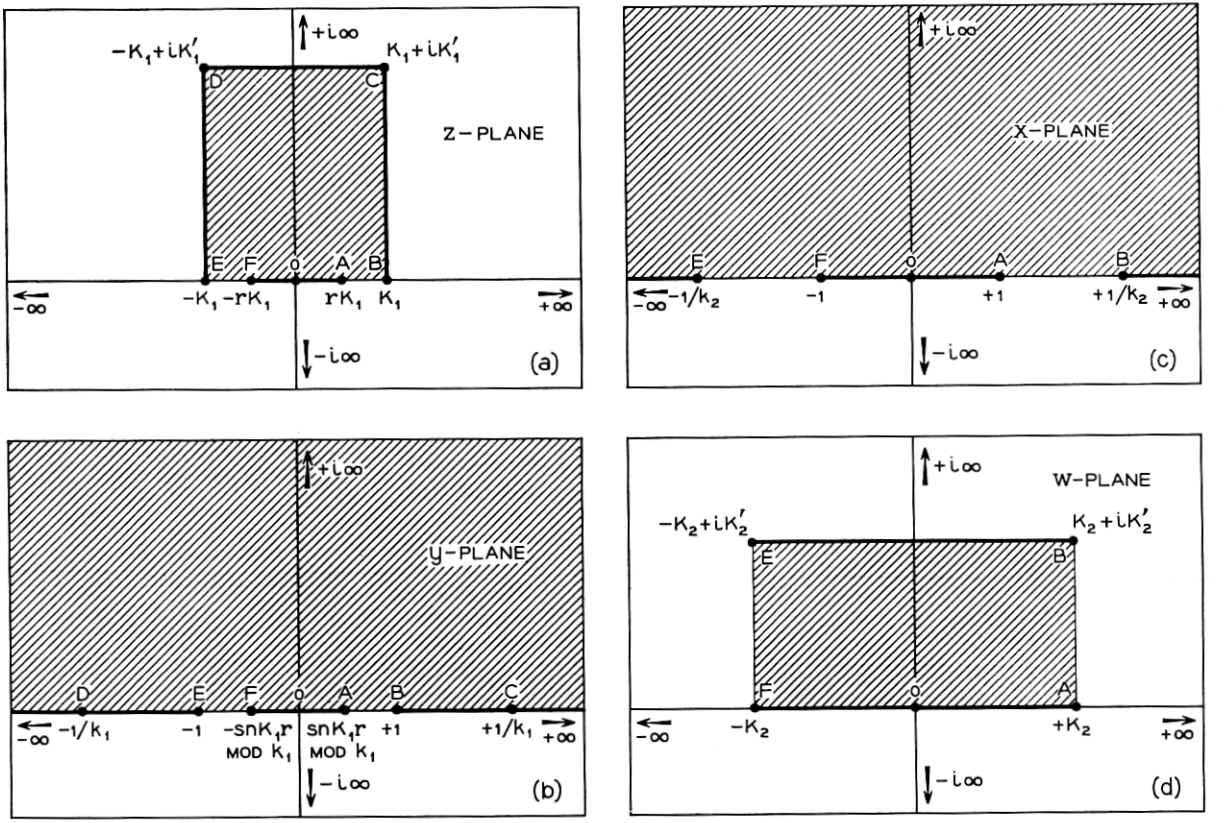

Fig. 20 — (a) Original electrode configuration of the upper cutoff frequency situation in the z plane. (b) Geometry after transformation into the upper half of the y plane. (c) Same geometry scaled in the x plane for subsequent

TABLE I — SUMMARY OF TRANSFORMATIONS FOR UPPER CUTOFF FREQUENCY CASE

	z	y	x	w
O	0	0	0	0
B	K_1	1	$1/(\text{sn } K_1 r \bmod k_1)$	$K_2 + iK_2'$
E	$-K_1$	-1	$-1/(\text{sn } K_1 r \bmod k_1)$	$-K_2 + iK_2'$
C	$K_1 + iK_2'$	$1/k_1$	not of interest	
D	$-K_1 + iK_1'$	$-1/k_1$		
A	$K_1 r$	$\text{sn } K_1 r \bmod k_1$	1	K_2
F	$-K_1 r$	$-\text{sn } K_1 r \bmod k_1$	-1	$-K_2$

$k_1 = \sin \theta_1$
$k_2 = \sin \theta_2$
$\theta_2 = \phi = \sin^{-1} [\text{sn } K_1 r \bmod k_1 \text{ or } \theta_1]$

Tables the Legendre notation (34), (35), (36), and (37) is used. Entering these tables with $z = K_1 r$ and the angle θ_r, a value of ϕ in radians is found. This value ϕ is converted to degrees and renamed θ_2.

(*b*) *From the y plane to the x plane.*

This is a change of scale and is accomplished by dividing all values by

$$\sin \phi = k_2 = \text{sn } K_1 r \bmod \theta_r . \tag{40}$$

After this step the arrangement of the points OBEAF on the real axis is the standard one for transformation of the upper half plane into a rectangle.

(*c*) *From the x plane to the w plane.*

This transformation finally shapes the original electrode geometry into the desired parallel plane geometry. The transformation is indicated in Table I. However, since the interest centers only on the impedance — that is, the length-dimension ratio of this final rectangle — it is not necessary to carry out this transformation in detail. This ratio $W'/D' = K_2'/2K_2$ is obtained from Fig. 19 by entering it with the modular angle $\theta_2 = \phi = \sin^{-1} k_2$.

Following these steps in the case $r = \frac{1}{2}$, the curve of Fig. 10 was obtained.

A short-cut is possible if $\theta_1 < 30°$; that is, if $W/D > 0.65$. In that case the sn function can be approximated by a sine function and $K \approx \pi/2$. Then $\phi = \theta_2 = r\pi/2$; in particular, for $r = \frac{1}{2}$, $\phi = \theta_2 = 45°$ and $W'/D' = \frac{1}{2}$.

A.4 *Mapping of the Lower Cutoff Frequency Configuration*

The procedure is quite similar to that used for the upper cutoff frequency geometry. It is summarized in Table II and Fig. 21.

TABLE II — SUMMARY OF TRANSFORMATIONS FOR LOWER CUTOFF FREQUENCY CASE

	z	y	x	w
O	0	0	0	0
B	K_1	1	not of interest	
E	$-K_1$	-1		
C	$K_1 + iK_1$	$1/k_1$	$1/(k_1 \text{ sn } K_1 r \bmod k_1)$	$K_2 + iK_2'$
D	$-K_1 + iK_1'$	$-1/k_1$	$-1/(k_1 \text{ sn } K_1 r \bmod k_1)$	$-K_2 + iK_2'$
A	rK_1	$\text{sn } K_1 r \bmod k_1$	1	K_2
F	$-rK_1$	$-\text{sn } K_1 r \bmod k_1$	-1	$-K_2$

$k_1 = \sin \theta_1$
$k_2 = \sin \theta_2$
$\theta_2 = \sin^{-1} [(\text{sn } K_1 r \times \sin \theta_1) \bmod k_1 \text{ or } \theta_1]$

(*a*) *From the z plane to the y plane.*

This step is identical to the first transformation of the upper cutoff frequency configuration.

(*b*) *From the y plane to the x plane.*

This scaling is also the same as that used before. The difference is, however, that now the points C and D are of interest, whereas before the points considered were B and E.

(*c*) *From the x plane to the w plane.*

Here the transformation differs; now a different modulus

$$k_2 = k_1 \text{ sn } K_1 r \bmod k_1$$

is used. The resulting complete integral values K_2 and K_2' are not to be confused with those obtained for the upper cutoff frequency case. Since the interest centers only on the impedance value $K_2'/2K_2 = W'/D'$ of the resulting rectangle, it is not necessary to evaluate this transformation in detail. The numerical evaluation is quite similar to the one of the upper cutoff situation. Using Fig. 19, one finds the first modular angle θ_1 from $K_1'/2K_1 = W/D$ of the original geometry. Entering the tables with $z = K_1 r$ and θ_1, an integral value ϕ is found. This value is obtained in radians. Then form

$$\begin{aligned} k_2 = \sin \theta_2 &= \sin \theta_1 \times (\text{sn } K_1 r \bmod k_1) \\ &= \sin \theta_1 \times (\sin \phi \bmod \theta_1). \end{aligned} \tag{41}$$

Using this formula, the angle θ_2 is evaluated in degrees. Then the graphs (Fig. 19) can be used again to obtain from θ_2 the length dimension ratio W'/D' of the transformed rectangle.

Following this procedure for the case $r = \frac{1}{2}$, the graph of Fig. 12 was obtained.

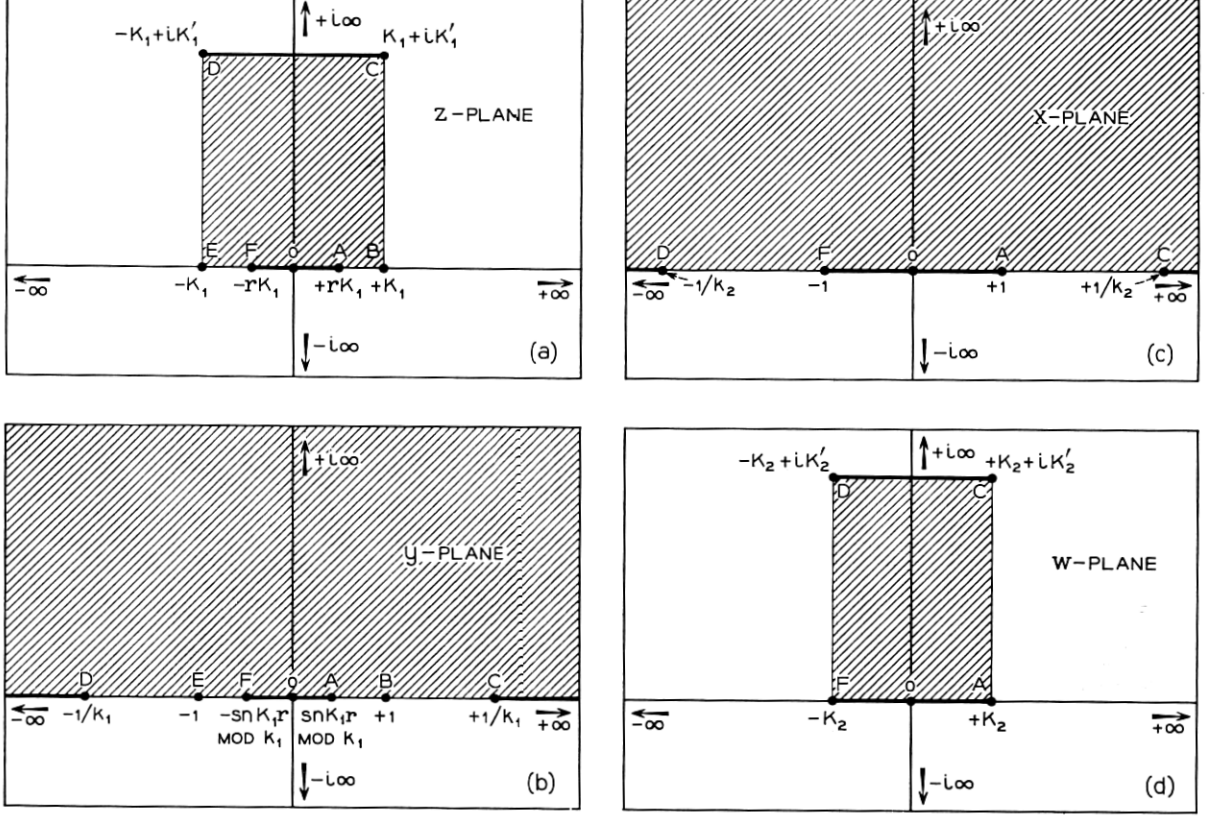

Fig. 21 — (a) Original electrode configuration corresponding to the lower cutoff frequency situation, shown in the z plane. (b) Geometry after transformation into the upper half of the y plane. (c) Same geometry scaled up in the x plane for subsequent transformation. (d) Electrode configuration transformed into a simple parallel plate geometry in the w plane.

REFERENCES

1. DeGrasse, R. W., Schulz-DuBois, E. O., and Scovil, H. E. D., Three-Level Solid-State Traveling Wave Maser, B.S.T.J., **38,** March, 1959, pp. 305–334.
2. Geusic, J. E., to be published.
3. Feher, G., Sensitivity Considerations in Microwave Paramagnetic Resonance Absorption Techniques, B.S.T.J., **36,** March, 1957, pp. 449–484.
4. DeGrasse, R. W., Kostelnick, J. J., and Scovil, H. E. D., Dual Channel 2390-mc Traveling-Wave Maser, B.S.T.J., **40,** July, 1961, pp. 1117–1128.
5. Harris, S. E., DeGrasse, R. W., and Schulz-DuBois, E. O., Solid State Maser Research, U. S. Signal Corps Report under Contract No. DA 36-039 SC-85357, First Quarterly Report, 20 September 1960. Available through ASTIA. Unpublished.
6. Tabor, W. J., and Sibilia, J. T., Masers for the *Telstar* Satellite Communications Experiment, B.S.T.J., **42,** July, 1963, pp. 1863–1886.
7. Hensel, M. L., and Treacy, E. B., to be published.